

**Figure 7.** FOXRED1-FLAG co-immunoprecipitates with a subset of complex I subunits. (A) Schematic representation of FOXRED1 co-immunoprecipitation approach.  $\Delta$ FOXRED1 cells were transfected with a construct encoding wild-type or inactive mutant p.Y359A FOXRED1, with and without a FLAG tag. Expression of FOXRED1 is able to restore levels of complex I subunits in both the tagged and untagged samples. FOXRED1 (denoted 'F') is able to bind to interacting partners (X represents an interacting protein while Y represents a protein required for

residues to investigate their role in FOXRED1 function and possible FAD binding. Tyrosine, cysteine and histidine residues are capable of being covalently flavinated, while tyrosine and phenylalanine are also capable of non-covalent stabilization of FAD through interactions with the phenyl moiety (42–44). Residues Y327, Y349 and Y359 were chosen based on high conservation within FOXRED1 in different species. Also, the predicted structural similarity of FOXRED1 with sarcosine oxidase (MSOX) (26) led us to select residues Y410 and Y411, as these two tyrosine residues align closely with the residue C316, the site of covalent attachment of FAD in MSOX (45). While mutations in residues Y327, Y349, Y410 and Y411 were able to restore complex I levels to that of wild-type cells, the mutation Y359A was not (Fig. 6D, lane 9). As the Y359F mutation was still functional (Fig. 6D, lane 8), it suggests that the phenyl moiety at position 359 is critical for the function of FOXRED1 in the biogenesis of complex I. Equal levels of expression were confirmed by SDS-PAGE and western blot analysis (Fig. 6D, bottom panel).

### FOXRED1 co-immunoprecipitates with a subset of complex I subunits

Given the lack of specific antibodies for FOXRED1, we were unable to determine whether the endogenous protein forms stable complexes. Furthermore, following ectopic expression of epitope-tagged FOXRED1 in control or  $\Delta$ FOXRED1 cells, we were unable to detect the presence of specific FOXRED1-containing complexes on BN-PAGE (data not shown). FOXRED1 may therefore transiently or loosely associate with complex I intermediates which are refractory to BN-PAGE. To investigate FOXRED1 interactions, we performed co-immunoprecipitation analysis of FOXRED1-FLAG expressed in  $\Delta$ FOXRED1 cells. In this case, we employed stable-isotope labeling of cells (SILAC) and subsequent quantitative mass spectrometry of eluted proteins (46,47). To correct for potential bias due reduced levels of complex I subunits in  $\Delta$ FOXRED1 mitochondria (Fig. 4), we also expressed FOXRED1 lacking the C-terminal FLAG epitope in  $\Delta$ FOXRED1 cells (see Fig. 7A for more details). In addition to this, we also performed co-immunoprecipitation analysis of the inactive FOXRED1<sup>Y359A</sup>-FLAG mutant in the same manner to determine proteins specifically bound to the functional FOXRED1 (Fig. 7A). As can be seen (Fig. 7B and C; Supplementary material, Tables S1 and S2), FOXRED1, but not the mutant FOXRED1<sup>Y359A</sup>, co-immunoprecipitated with a number of complex I subunits including NDUFB10,

import or biogenesis) while contaminating proteins (A) bind non-specifically to the resin in all cases. Upon washing and elution, FOXRED1-containing complexes are enriched in FLAG-tagged elutions while contaminating proteins elute in all samples. Following SILAC analysis, contaminating proteins are removed, while true FOXRED1-binding proteins are enriched. (B) Mitochondria from heavy or light amino acid-labeled  $\Delta$ FOXRED1 cells expressing FOXRED1 or FOXRED1<sup>FLAG</sup> were subjected to immunoprecipitation with anti-FLAG beads. Elutions were mixed and analyzed by LC-MS. The means of normalized heavy/light ratios ( $\log_{10}$ ), identified in at least two replicates (including a label switch;  $N = 4$ ) were plotted against their  $P$ -values ( $-\log_{10}$ ). Thresholds were set at  $P$ -values  $< 0.05$  and mean heavy/light enrichment ratios  $> 6$ . For simplicity, only bona fide mitochondrial proteins present in the MitoCarta dataset are shown, and commonly used protein names are substituted for gene names (Hsp10, HSP60, HSPD1; mt-Hsp70, HSPA9; Miro-2, RHOT2; MPPalpha, PMPCA; MPPbeta, PMPCB; Tim8a, TIMM8A; Tim13, TIMM13; Tom20, TOMM20; Tom22, TOMM22). Unfiltered data can be found in Supplementary material, Table S1. (C) Mitochondria from heavy or light amino acid-labeled HEK293T cells expressing FOXRED1<sup>Y359A</sup> or FLAG-tagged FOXRED1<sup>Y359A</sup> were subjected to anti-FLAG immunoprecipitation and analysis performed as in (A). Unfiltered data can be found in Supplementary material, Table S2.

NDUFS5, NDUFA10, NDUFA8, NDUFS3 and NDUFA5. The potential association of FOXRED1 with components of the import machinery (e.g. Tom20, Tom22 and MPP) and chaperones (e.g. mtHsp70 and Hsp60/10) may be related to the biogenesis of FOXRED1 due to its ectopic expression. Importantly, we did not observe specific association with subunits of the other respiratory chain complexes, indicating that the interactions are specific and are likely to occur at stages in assembly prior to assembly of complex I intermediates into respirasomes (48).

## Discussion

### Loss of FOXRED1 leads to impaired complex I assembly and the presence of a crippled subassembly

While it has been established that FOXRED1 is involved in complex I biogenesis (24) and mutations in its gene cause mitochondrial disease related to complex I deficiency (25,26), little information is available regarding its functional role. Here we found that FOXRED1 associates with the matrix side of the inner membrane, following import of the protein in a membrane potential-dependent manner, and interacts with a subset of complex I subunits. Moreover, loss of FOXRED1 leads to defects in the latter stages of complex I assembly, resulting in the accumulation of a crippled ~475 kDa subcomplex. We believe that this ~475 kDa subcomplex represents a non-productive breakdown of a stalled assembly intermediate for the following reasons. First, pulse-chase assembly analysis indicated that at early time points, FOXRED1 patient cell mitochondria could form a late stage ~815 kDa complex I intermediate, but this was unproductive, and was followed by the formation of the ~475 kDa complex. Confirmation that this was the ~815 kDa intermediate was demonstrated by its association with the assembly factor NDUFAP1. In addition, the ~475 kDa complex was no longer associated with NDUFAP1. Secondly, the ~475 kDa complex contained most, if not all, mtDNA-encoded complex I subunits, indicating that the hydrophobic arm was largely intact. The reasons for such instability of the ~815 kDa intermediate are not clear, but similar observations have been seen in cells lacking the NDUFA9 subunit ( $\Delta$ NDUFA9) that sits at the interface between the matrix and membrane arms of complex I (33). Indeed, the unproductive complex observed in  $\Delta$ NDUFA9 mitochondria also contained the late assembly subunit NDUFS5, suggesting the unproductive complex to also be a breakdown product of the ~815 kDa complex.

The late stage ~815 kDa complex also interacts with various assembly factors including NDUFAP1, Ecsit, ACAD9 and other proteins that form the MC1A complex (23), as well as NDUFAP2, which stabilizes the assembly in the absence of N-module subunits (49). Given the involvement of multiple assembly factors converging at this point, and our observation that loss of FOXRED1 leads to instability and breakdown of the ~815 kDa species, this suggests that the late stages of complex I assembly represent a critical nexus in the enzyme's biogenesis.

### FOXRED1 is found in association with complex I subunits

The exact molecular role played by FOXRED1 still remains unclear, but this is also the case for many complex I assembly factors that have been identified in the past decade (19). FOXRED1 has putative oxidoreductase activity and has homology to FAD-binding proteins that are involved in redox reactions related to amino acid catabolism (dimethylglycine dehydrogenase, sarcosine dehydrogenase, L-pipecolic acid oxidase and peroxisomal sarcosine oxidase) and metabolic regulation (pyruvate

dehydrogenase regulatory subunit) (25,26). However, there is still no direct evidence for FAD-binding or oxidoreductase activity. Mutations of residues involved in potential FAD binding did not result in inhibition in FOXRED1 activity, except for the substitution of Tyr359 for Ala. It remains to be determined whether this mutation leads to potential defects in FAD binding, or if it causes other defects, such as impairing protein folding. Nevertheless, this construct served as a useful control to determine the proteins that can form a complex with FOXRED1.

The recent determination of a 5 Å cryo-EM structure of bovine complex I revealed not only conservation of the core subunits from *T. thermophilus* but also the presence of density attributed to the accessory subunits (2). This structure revealed that the subunits identified as co-immunoprecipitating with FOXRED1 (NDUFS3, NDUFA10 and NDUFA5) are located in close proximity to each other and to the mitochondrial inner membrane, consistent with the sub-mitochondrial localization of FOXRED1. Furthermore, HA-tagged NDUFS5 has been found in association with FOXRED1 (23), while FOXRED1 was also identified in stalled complex I subcomplexes lacking NDUFA11 (32). Together, these data suggest that FOXRED1 may function in a complex comprising at least the core subunit NDUFS3 and the accessory subunits NDUFA5, NDUFA10, NDUFB10 and NDUFS5. Proteomic analysis failed to detect any subunits of other respiratory complexes, suggesting FOXRED1 performs its function prior to incorporation of complex I intermediates with other respiratory complexes. Assembly of complex I with other complexes has been suggested to occur following assembly of the ~815 kDa subcomplex, and before assembly into holocomplex I (39,48). Because we are unable to identify subunits belonging to other respiratory complexes, we can conclude that FOXRED1 most likely exerts its function prior to this stage, thus being a mid-stage assembly factor for the biogenesis of complex I.

### FOXRED1 patient mutations remain partially functional

Two separate missense mutations in FOXRED1, resulting in the substitutions p.R352W (26) and p.N430S (25), lead to loss of complex I activity and mitochondrial disease. Most patients with nuclear gene defects and complex I dysfunction display severe symptoms and do not survive to adulthood (21). Interestingly, both patients harboring FOXRED1 mutations survived to adulthood. This indicates that the mutations result in partial loss of function and/or loss of FOXRED1 can be compensated by other factors. Our studies indicate that the former is most likely true since total loss of FOXRED1 leads to severe reduction in complex I levels while overexpression of either of the mutant forms in these cells restores complex I. Thus, the pathogenic mutations in FOXRED1 are most likely hypomorphic in nature. Similar observations have also been for the complex I assembly factor NUBPL where overexpression of a p.Gly56Arg missense mutation could overcome a complex I defect in patient cell lines (50). It is therefore possible that future therapeutic treatments could involve mechanisms to increase the synthesis of these mutant proteins so that the reduced assembly activity is dampened. Current therapies for complex I deficiency and mitochondrial disease include supplementation with various metabolites such as dichloroacetate, CoQ<sub>10</sub>, creatine or riboflavin (51,52). While symptoms may improve for some patients, it has been shown that responsiveness may depend on the particular gene mutation present, leading to a non-responsive phenotype (53,54). Our data suggest that future therapies could include the identification of pharmacological agents that enhance expression of the mutant protein, thereby overcoming effects of pathological mutations and restoring levels of complex I.

## Materials and Methods

### Cloning and molecular biology

The FOXRED1 open reading frame was amplified from a cDNA library and cloned into the pGEM4Z vector (Promega, Madison, WI, USA) for import studies and also in frame with a C-terminal FLAG epitope containing pCDNA3 vector for expression studies. Site-directed mutagenesis was performed using the Phusion mutagenesis method (New England Biolabs) according to manufacturers' instructions.

For TALEN construction, the 5' UTR and first exon of human FOXRED1 (NM\_017547) was used as the input sequence for designing suitable TALEN-binding pairs using the ZiFiT Targeter Version 4.2 (16). The binding pair FOXRED1-L (NG HD NI NN NI NN NN NN NG HD HD NN NN NN HD NG HD) and FOXRED1-R (NG NN HD HD NN NG NN HD NN NN HD NI NN NI NI HD HD) were, respectively, assembled into the JDS70 (NI) and JDS71 (HD) backbones, yielding pTALEN-FOXRED1-L and pTALEN-FOXRED1-R, according to Reyon *et al.* (55).

### Cell culture

Patient and control fibroblasts used in this study have been reported previously (25). Generation and genomic verification of the  $\Delta$ FOXRED1 cell lines was performed according to Stroud *et al.* (33). Isogenic HEK293T cells were used as a control. Cells were cultured in DMEM supplemented with 10% (v/v) fetal bovine serum (FBS) and penicillin/streptomycin with 50  $\mu$ g/ml uridine. Cells were grown at 37°C under an atmosphere of 5% CO<sub>2</sub>. For cell viability measurements, cells were grown in glucose or galactose-containing media for 72 h before harvesting adherent and non-adherent cells and staining with 0.2% trypan blue. Cells (>300/sample) were subsequently counted.

For SILAC, cells were cultured in SILAC DMEM (Thermo-Fisher Scientific; 4.5 g/l glucose, 4 mM L-glutamine, 110 mg/l sodium pyruvate) containing 10% (v/v) dialyzed FBS, supplemented with penicillin/streptomycin, 50  $\mu$ g/ml uridine, 600 mg/l L-proline and either 'light' amino acids (146 mg/l L-lysine-HCl and 42 mg/l L-arginine-HCl), or 'heavy' amino acids (180 mg/l <sup>13</sup>C<sub>6</sub><sup>15</sup>N<sub>2</sub>-L-lysine-2HCl and 44 mg/l <sup>13</sup>C<sub>6</sub><sup>15</sup>N<sub>4</sub>-L-arginine-HCl; Cambridge Isotope Laboratories). All cells were cultured at 37°C under 5% CO<sub>2</sub>, 95% air.

### Complementation studies

For the lentiviral-mediated rescue of patient fibroblasts, the FOXRED1 open reading frame was cloned into the pGEM4Z vector (Promega) and then subcloned into the 4-hydroxytamoxifen-inducible lentiviral vector pF-5X-UAS-MCS-SV40-puroGal4ER<sup>T2</sup>VP16 (GEV16)-W as described in (31). Lentiviral particles were generated and infected into cells as previously described (31,38). Following 20 days of selection, FOXRED1 expression was induced by addition of 100 nM 4HT to the media, and cells were then harvested for western blotting analysis. For complementation of  $\Delta$ FOXRED1 cells, pCDNA3 plasmid containing FLAG-tagged wild-type or mutant FOXRED1 was transfected using Lipofectamine 2000 according to manufacturer's instructions (Invitrogen). The following day, media was refreshed and cells grown an additional 48 h prior to analysis.

### Mitochondrial localization analysis

Mitochondria were isolated according to the methods of Johnston *et al.* (41). For subfractionation, mitochondria were resuspended in

either 10 mM MOPS (pH 7.2) and 250 mM sucrose or 10 mM MOPS (pH 7.2), and treated with 0.1 mg/ml proteinase K for 30 min on ice (27). Alternatively, isolated mitochondria were subjected to either sonication in 100 mM NaCl and 10 mM Tris-HCl (pH 7.6) or alkaline extraction in freshly prepared 0.1 M Na<sub>2</sub>CO<sub>3</sub> (pH 11.5). Membranes were pelleted at 100 000g for 30 min at 4°C, and supernatants were precipitated with trichloroacetic acid (27). After treatments, soluble (supernatant) and insoluble (pellet) fractions were subjected to SDS-PAGE and western blot analysis.

### Radiolabeling studies

mtDNA-encoded translation products were labeled using previously described methods (56). For import studies, radiolabeled FOXRED1 was translated using TnT Coupled Reticulocyte Lysate (Promega) in the presence of a [<sup>35</sup>S]-methionine/cysteine. Translated protein was incubated with mitochondria isolated from HEK293T cells at 37°C for various times. Proteinase K treatment and dissipation of membrane potential were performed as described elsewhere (39).

### Co-immunoprecipitation analysis

For immunoprecipitation, SILAC-labeled  $\Delta$ FOXRED1 cells were transfected with pCDNA3 plasmid harboring DNA encoding FOXRED1-FLAG, FOXRED1, FOXRED1<sup>Y359A</sup>-FLAG or FOXRED1<sup>Y359A</sup> and allowed to express protein for 48 h. Mitochondria were then isolated and solubilized in lysis buffer (20 mM Bis-Tris, pH 7, 50 mM NaCl, 10% glycerol) containing 1% (w/v) digitonin. Individual lysates were incubated with anti-FLAG M2 affinity gel (Sigma) for 2 h at 4°C with gentle rotation. Following washing with lysis buffer containing 0.1% (w/v) digitonin, bound protein was eluted with 100  $\mu$ g/ml FLAG peptide (Sigma).

### Mass spectrometry and data analysis

Proteins were acetone precipitated, solubilized in 8 M urea, 0.05% ProteaseMax (Promega), 50 mM ammonium bicarbonate, and reduced and alkylated with 5 mM Tris(2-carboxyethyl)phosphine hydrochloride and 50 mM iodoacetamide at 37°C for 30 min. Proteins were digested with LysC (Promega) at 37°C for 2 h, followed by dilution of the solution to 2 M urea and continuation of the digestion continued at 37°C overnight with the addition of Trypsin (Promega). The digest was acidified with 1% (v/v) trifluoroacetic acid (TFA) and the peptides desalted on SDB-XC (Empore) Stage-Tips as previously described (57). Peptides were analyzed by an online nano-HPLC/electrospray ionization-MS/MS on an LTQ-Orbitrap Elite Instrument connected to an Ultimate 3000 HPLC (Thermo-Fisher Scientific). Peptides reconstituted in 0.1% TFA and 2% acetonitrile (ACN) were loaded onto a trap column (C<sub>18</sub> PepMap 100  $\mu$ m ID  $\times$  2 cm trapping column, Thermo-Fisher Scientific) at 5  $\mu$ l/min for 6 min, and washed for 6 min before switching the precolumn in line with the analytical column (Vydac MS C<sub>18</sub>, 3  $\mu$ m, 300 Å and 75  $\mu$ m ID  $\times$  25 cm, Grace Pty. Ltd.). The separation of peptides was performed at 300 nl/min using a non-linear ACN gradient of buffer A (0.1% formic acid, 2% ACN) and buffer B (0.1% formic acid, 80% ACN), starting at 5% buffer B to 55% over 120 min. Data were collected in Data-Dependent Acquisition mode using m/z 350–1500 as MS scan range, CID for MS/MS of the 20 most intense ions. Other instrument parameters were: MS scan at 120 000 resolution, maximum injection time 150 ms, AGC target 1E<sup>6</sup>, CID at 35% energy for a maximum injection time of 150 ms with AGC target of 5000.

For data analysis, Thermo MS raw files were analyzed using the MaxQuant platform (version 1.5.0.30); (58) searching against the human UniProt FASTA database (release 38 July 2014; 88993 entries) and a database containing common contaminants by the Andromeda search engine (59). Default setting parameters were used with modifications. Briefly, cysteine carbamidomethylation was used as a fixed modification, and N-terminal acetylation and methionine oxidation were used as variable modifications. False discovery rates of 1% for proteins and peptides were applied by searching a reverse database, and 'Re-quantify' and 'Match between runs' options were enabled. Unique and razor peptides were used for quantification, using a minimum ratio count of 1. Data analysis was performed using the Perseus software. SILAC ratios (heavy/light) were filtered for proteins quantified by >1 unique peptide and >5% sequence coverage. Mean normalized ratios were calculated from each of these proteins identified in >2/4 replicates and  $\log_{10}$  transformed. P-values across replicates were calculated by a one-tailed t-test. Gene names were matched to gene symbols and synonyms listed in the human MitoCarta dataset (24).

### Oxygen consumption and enzyme activity measurements

OCRs and ECARs were measured in live cells using a Seahorse Biosciences XF24-3 Analyzer according to manufacturer's procedures. Briefly, 50 000 HEK293T cells were plated per well of a poly-D-lysine-treated Seahorse Biosciences culture plate and grown overnight in standard culture conditions. OCR and ECAR were analyzed in cells in non-buffered media with the following inhibitors: 2  $\mu\text{M}$  oligomycin, 0.5  $\mu\text{M}$  carbonyl cyanide 4-(trifluoromethoxy) phenylhydrazone (FCCP), and 0.3  $\mu\text{M}$  antimycin A along with 0.5  $\mu\text{M}$  rotenone. Four measurement cycles (2 min mix, 2 min wait, 5 min measure) were done for basal conditions, and following each inhibitor injection. For each cell line, 7–10 replicate wells were measured in triplicate plates and measurements normalized to cell number with CyQuant (Life Technologies). Basal ECAR, basal OCR and non-mitochondrial respiration were calculated as an average of the four measurement points. Basal mitochondrial OCR was determined from basal OCR minus non-mitochondrial respiration rate. To calculate proton leak and maximal respiration, the initial measurement following addition of oligomycin or FCCP, respectively, was used. The activity of OXPHOS complexes I–IV and citrate synthase (CS) were measured in enriched mitochondrial preparations from cells with (CI, CII, CIV and CS) and without (CIII) hypotonic treatment, as described by Frazier and Thorburn (60).

### SDS-PAGE, BN-PAGE and western blot analysis

SDS-PAGE was performed using Tris-Tricine gradient gels (61) and BN-PAGE and second dimension SDS-PAGE was performed according to Lazarou *et al.* (39). BN-PAGE molecular-weight markers employed were thyroglobulin (669 kDa), ferritin (440 kDa) and BSA (137 and 67 kDa) and were employed as reference markers rather than true size estimations. In-gel activity assays were performed according to Zerbetto *et al.* (62). Antibodies were purchased for NDUFS2, NDUFS3, SDHA, Core I and COXIV (Sapphire Biosciences), COII (Invitrogen), NDUFV2 and FLAG-epitope (Sigma), Tom20 (Santa Cruz, CA, USA), Tim23 and cytochrome c (BD Transduction Laboratories), while rabbit polyclonal GFP, NDUFA9, NDUFB6, NDUFS5, NDUFAF1, NDUFAF2, NDUFAF4, Ecsit, mtHsp70 and ACAD9 were made in-house. The ND1 antibody was a gift from A. Lombès (Paris, France). Secondary probing with  $\alpha$ -mouse

or  $\alpha$ -rabbit horseradish-peroxidase-conjugated antibodies (Sigma) was performed for 2 h, followed by detection using Enhanced Chemiluminescence reagents (GE Healthcare, NJ, USA) and a ChemiDoc Imaging system (Bio-Rad, Hercules, CA, USA).

### Supplementary Material

Supplementary Material is available at HMG online.

### Acknowledgements

We thank Wendy Wang and Christa George for technical assistance, Boris Reljic for discussions and Ann Lombès for the ND1 antibody.

Conflict of Interest statement: None declared.

### Funding

This work was supported by Australian National Health and Medical Research Council grants (to M.T.R., D.A.S. and D.R.T.) and Fellowships (Early Career Fellowship to D.A.S., Career Development Fellowship to A.E.F., Principal Research Fellowship to D.R.T.), Australian Research Council Future Fellowship (to M.Mc.K.), the Australian Mitochondrial Disease Foundation (AMDF), the Victorian Government's Operational Infrastructure Support Program and JSPS KAKENHI (Grant number 25461539 to M.M.).

### References

- Brandt, U. (2006) Energy converting NADH:quinone oxidoreductase (complex I). *Annu. Rev. Biochem.*, **75**, 69–92.
- Vinothkumar, K.R., Zhu, J. and Hirst, J. (2014) Architecture of mammalian respiratory complex I. *Nature*, **515**, 80–84.
- Wittig, I., Carozzo, R., Santorelli, F.M. and Schagger, H. (2006) Supercomplexes and subcomplexes of mitochondrial oxidative phosphorylation. *Biochim. Biophys. Acta*, **1757**, 1066–1072.
- Kirby, D.M., Crawford, M., Cleary, M.A., Dahl, H.H., Dennett, X. and Thorburn, D.R. (1999) Respiratory chain complex I deficiency: an underdiagnosed energy generation disorder. *Neurology*, **52**, 1255–1264.
- Triepels, R.H., Van Den Heuvel, L.P., Trijbels, J.M. and Smeitink, J.A. (2001) Respiratory chain complex I deficiency. *Am. J. Med. Genet.*, **106**, 37–45.
- Schapira, A.H., Cooper, J.M., Dexter, D., Clark, J.B., Jenner, P. and Marsden, C.D. (1990) Mitochondrial complex I deficiency in Parkinson's disease. *J. Neurochem.*, **54**, 823–827.
- Latha, D., Vijayendran, R., Badanavala, M.P., Narayan, G.A. and Hindupur, K.A. (2008) Mitochondrial import and accumulation of  $\alpha$ -synuclein impair complex I in human dopaminergic neuronal cultures and parkinson disease brain. *J. Biol. Chem.*, **283**, 9089–9100.
- Miwa, S., Jow, H., Baty, K., Johnson, A., Czapiewski, R., Saretzki, G., Treumann, A. and von Zglinicki, T. (2014) Low abundance of the matrix arm of complex I in mitochondria predicts longevity in mice. *Nat. Commun.*, **5**, 3837.
- Carroll, J., Fearnley, I.M., Shannon, R.J., Hirst, J. and Walker, J.E. (2003) Analysis of the subunit composition of complex I from bovine heart mitochondria. *Mol. Cell. Proteomics*, **2**, 117–126.
- Carroll, J., Fearnley, I.M., Skehel, J.M., Shannon, R.J., Hirst, J. and Walker, J.E. (2006) Bovine complex I is a complex of 45 different subunits. *J. Biol. Chem.*, **281**, 32724–32727.

11. Balsa, E., Marco, R., Perales-Clemente, E., Szklarczyk, R., Calvo, E., Landazuri, M.O. and Enriquez, J.A. (2012) NDUFA4 is a subunit of complex IV of the mammalian electron transport chain. *Cell Metab.*, **16**, 378–386.
12. Hirst, J., Carroll, J., Fearnley, I.M., Shannon, R.J. and Walker, J.E. (2003) The nuclear encoded subunits of complex I from bovine heart mitochondria. *Biochim. Biophys. Acta*, **1604**, 135–150.
13. Stojanovski, D., Johnston, A.J., Streimann, I., Hoogenraad, N.J. and Ryan, M.T. (2003) Import of nuclear-encoded proteins into mitochondria. *Exp. Physiol.*, **88**, 57–64.
14. Hoogenraad, N.J., Ward, L.A. and Ryan, M.T. (2002) Import and assembly of proteins into mitochondria of mammalian cells. *Biochim. Biophys. Acta*, **1592**, 97–105.
15. Janssen, R.J., Nijtmans, L.G., van den Heuvel, L.P. and Smeitink, J.A. (2006) Mitochondrial complex I: structure, function and pathology. *J. Inherit. Metab. Dis.*, **29**, 499–515.
16. Lazarou, M., Thorburn, D.R., Ryan, M.T. and McKenzie, M. (2009) Assembly of mitochondrial complex I and defects in disease. *Biochim. Biophys. Acta*, **1793**, 78–88.
17. McKenzie, M. and Ryan, M.T. (2010) Assembly factors of human mitochondrial complex I and their defects in disease. *IUBMB Life*, **62**, 497–502.
18. Schultz, B.E. and Chan, S.I. (2001) Structures and proton-pumping strategies of mitochondrial respiratory enzymes. *Annu. Rev. Biophys. Biomol. Struct.*, **30**, 23–65.
19. Mimaki, M., Wang, X., McKenzie, M., Thorburn, D.R. and Ryan, M.T. (2012) Understanding mitochondrial complex I assembly in health and disease. *Biochim. Biophys. Acta*, **1817**, 851–862.
20. Ugalde, C., Vogel, R., Huijbens, R., Van Den Heuvel, B., Smeitink, J. and Nijtmans, L. (2004) Human mitochondrial complex I assembles through the combination of evolutionary conserved modules: a framework to interpret complex I deficiencies. *Hum. Mol. Gen.*, **13**, 2461–2472.
21. Nouws, J., Nijtmans, L.G., Smeitink, J.A. and Vogel, R.O. (2012) Assembly factors as a new class of disease genes for mitochondrial complex I deficiency: cause, pathology and treatment options. *Brain*, **135**, 12–22.
22. Heide, H., Bleier, L., Steger, M., Ackermann, J., Drose, S., Schwamb, B., Zornig, M., Reichert, A.S., Koch, I., Wittig, I. et al. (2012) Complexome profiling identifies TMEM126B as a component of the mitochondrial complex I assembly complex. *Cell Metab.*, **16**, 538–549.
23. Guarani, V., Paulo, J., Zhai, B., Huttlin, E.L., Gygi, S.P. and Harper, J.W. (2014) TIMMDC1/C3orf1 functions as a membrane-embedded mitochondrial complex I assembly factor through association with the MCIA complex. *Mol. Cell Biol.*, **34**, 847–861.
24. Pagliarini, D.J., Calvo, S.E., Chang, B., Sheth, S.A., Vafai, S.B., Ong, S.E., Walford, G.A., Sugiana, C., Boneh, A., Chen, W.K. et al. (2008) A mitochondrial protein compendium elucidates complex I disease biology. *Cell*, **134**, 112–123.
25. Calvo, S.E., Tucker, E.J., Compton, A.G., Kirby, D.M., Crawford, G., Burtt, N.P., Rivas, M., Guiducci, C., Bruno, D.L., Goldberger, O.A. et al. (2010) High-throughput, pooled sequencing identifies mutations in NUBPL and FOXRED1 in human complex I deficiency. *Nat. Gen.*, **42**, 851–858.
26. Fassone, E., Duncan, A.J., Taanman, J.W., Pagnamenta, A.T., Sadowski, M.I., Holand, T., Qasim, W., Rutland, P., Calvo, S.E., Mootha, V.K. et al. (2010) FOXRED1, encoding an FAD-dependent oxidoreductase complex-I-specific molecular chaperone, is mutated in infantile-onset mitochondrial encephalopathy. *Hum. Mol. Gen.*, **19**, 4837–4847.
27. Ryan, M.T., Voos, W. and Pfanner, N. (2001) Assaying protein import into mitochondria. *Methods Cell Biol.*, **65**, 189–215.
28. Jarvis, J.A., Ryan, M.T., Hoogenraad, N.J., Craik, D.J. and Høj, P.B. (1995) Solution structure of the acetylated and noncleavable mitochondrial targeting signal of rat chaperonin 10. *J. Biol. Chem.*, **270**, 1323–1331.
29. Walker, J.E., Arizmendi, J.M., Dupuis, A., Fearnley, I.M., Finel, M., Medd, S.M., Pilkington, S.J., Runswick, M.J. and Skehel, J.M. (1992) Sequences of 20 subunits of NADH:ubiquinone oxidoreductase from bovine heart mitochondria. Application of a novel strategy for sequencing proteins using the polymerase chain reaction. *J. Mol. Biol.*, **226**, 1051–1072.
30. Bolender, N., Sickmann, A., Wagner, R., Meisinger, C. and Pfanner, N. (2008) Multiple pathways for sorting mitochondrial precursor proteins. *EMBO Rep.*, **9**, 42–49.
31. Dunning, C.J.R., McKenzie, M., Sugiana, C., Lazarou, M., Silke, J., Connelly, A., Fletcher, J.M., Kirby, D.M., Thorburn, D.R. and Ryan, M.T. (2007) Human CIA30 is involved in the early assembly of mitochondrial complex I and mutations in its gene cause disease. *EMBO J.*, **26**, 3227–3237.
32. Andrews, B., Carroll, J., Ding, S., Fearnley, I.M. and Walker, J.E. (2013) Assembly factors for the membrane arm of human complex I. *Proc. Natl. Acad. Sci. USA*, **110**, 18934–18939.
33. Stroud, D., Formosa, L., Wijeyeratne, X., Nguyen, T. and Ryan, M. (2013) Gene knockout using transcription activator-like effector nucleases (TALENs) reveals that human NDUFA9 protein is essential for stabilizing the junction between membrane and matrix arms of complex I. *J. Biol. Chem.*, **288**, 1685–1690.
34. Perales-Clemente, E., Fernández-Vizcarra, E., Acín-Pérez, R., Movilla, N., Bayona-Bafaluy, M.P., Moreno-Loshuertos, R., Pérez-Martos, A., Fernández-Silva, P. and Enriquez, J.A. (2010) Five entry points of the mitochondrially encoded subunits in mammalian complex I assembly. *Mol. Cell Biol.*, **30**, 3038–3047.
35. Rhein, V.F., Carroll, J., Ding, S., Fearnley, I.M. and Walker, J.E. (2013) NDUFAF7 methylates arginine 85 in the NDUFS2 subunit of human complex I. *J. Biol. Chem.*, **288**, 33016–33026.
36. Zurita Rendón, O., Silva Neiva, L., Sasarman, F. and Shoubridge, E.A. (2014) The arginine methyltransferase NDUFAF7 is essential for complex I assembly and early vertebrate embryogenesis. *Hum. Mol. Genet.*, **23**, 5159–5170.
37. Sugiana, C., Pagliarini, D.J., McKenzie, M., Kirby, D.M., Salemi, R., Abu-Amero, K.K., Dahl, H.H., Hutchison, W.M., Vascotto, K.A., Smith, S.M. et al. (2008) Mutation of C20orf7 disrupts complex I assembly and causes lethal neonatal mitochondrial disease. *Am. J. Hum. Genet.*, **83**, 468–478.
38. McKenzie, M., Tucker, E.J., Compton, A.G., Lazarou, M., George, C., Thorburn, D.R. and Ryan, M.T. (2011) Mutations in the gene encoding C8orf38 block complex I assembly by inhibiting production of the mitochondria-encoded subunit ND1. *J. Mol. Biol.*, **414**, 413–426.
39. Lazarou, M., McKenzie, M., Ohtake, A., Thorburn, D.R. and Ryan, M.T. (2007) Analysis of the assembly profiles for mitochondrial- and nuclear-DNA-encoded subunits into complex I. *Mol. Cell Biol.*, **27**, 4228–4237.
40. Vogel, R.O., Janssen, R.J., Ugalde, C., Grovenstein, M., Huijbens, R.J., Visch, H.J., van den Heuvel, L.P., Willems, P.H., Zeviani, M., Smeitink, J.A. et al. (2005) Human mitochondrial complex I assembly is mediated by NDUFAF1. *FEBS J.*, **272**, 5317–5326.
41. Johnston, A.J., Hoogenraad, J., Dougan, D.A., Truscott, K.N., Yano, M., Mori, M., Hoogenraad, N.J. and Ryan, M.T. (2002) Insertion and assembly of human tom7 into the preprotein

- translocase complex of the outer mitochondrial membrane. *J. Biol. Chem.*, **277**, 42197–42204.
42. Zhou, B.P., Wu, B., Kwan, S.-W. and Abell, C.W. (1998) Characterization of a highly conserved FAD-binding site in human monoamine oxidase B. *J. Biol. Chem.*, **273**, 14862–14868.
  43. Ma, J. and Ito, A. (2002) Tyrosine residues near the FAD binding site are critical for FAD binding and for the maintenance of the stable and active conformation of rat monoamine oxidase A. *J. Biochem.*, **131**, 107–111.
  44. Mewies, M., McIntire, W.S. and Scrutton, N.S. (1998) Covalent attachment of flavin adenine dinucleotide (FAD) and flavin mononucleotide (FMN) to enzymes: the current state of affairs. *Protein Sci.*, **7**, 7–20.
  45. Trickey, P., Wagner, M.A., Jorns, M.S. and Mathews, F.S. (1999) Monomeric sarcosine oxidase: structure of a covalently flavinylated amine oxidizing enzyme. *Structure*, **7**, 331–345.
  46. Oeljeklaus, S., Schummer, A., Suppanz, I. and Warscheid, B. (2014) SILAC labeling of yeast for the study of membrane protein complexes. *Methods Mol. Biol.*, **1188**, 23–46.
  47. Ong, S.-E.E., Blagoev, B., Kratchmarova, I., Kristensen, D.B., Steen, H., Pandey, A. and Mann, M. (2002) Stable isotope labeling by amino acids in cell culture, SILAC, as a simple and accurate approach to expression proteomics. *Mol. Cell. Proteomics*, **1**, 376–386.
  48. Moreno-Lastres, D., Fontanesi, F., García-Consuegra, I., Martín, M.A., Arenas, J., Barrientos, A. and Ugalde, C. (2012) Mitochondrial complex I plays an essential role in human respirasome assembly. *Cell Metab.*, **15**, 324–335.
  49. Ogilvie, I., Kennaway, N.G. and Shoubridge, E.A. (2005) A molecular chaperone for mitochondrial complex I assembly is mutated in a progressive encephalopathy. *J. Clin. Invest.*, **115**, 2784–2792.
  50. Tucker, E.J., Mimaki, M., Compton, A.G., McKenzie, M., Ryan, M.T. and Thorburn, D.R. (2012) Next-generation sequencing in molecular diagnosis: NUBPL mutations highlight the challenges of variant detection and interpretation. *Hum. Mut.*, **33**, 411–418.
  51. Kerr, D.S. (2010) Treatment of mitochondrial electron transport chain disorders: a review of clinical trials over the past decade. *Mol. Genet. Metab.*, **99**, 246–255.
  52. DiMauro, S. and Rustin, P. (2009) A critical approach to the therapy of mitochondrial respiratory chain and oxidative phosphorylation diseases. *Biochim. Biophys. Acta*, **1792**, 1159–1167.
  53. Haack, T.B., Danhauser, K., Haberberger, B., Hoser, J., Strecker, V., Boehm, D., Uziel, G., Lamantea, E., Invernizzi, F., Poulton, J. et al. (2010) Exome sequencing identifies ACAD9 mutations as a cause of complex I deficiency. *Nat. Genet.*, **42**, 1131–1134.
  54. Nouws, J., Wibrand, F., van den Brand, M., Venselaar, H., Duno, M., Lund, A.M., Trautner, S., Nijtmans, L. and Ostergard, E. (2014) A patient with complex I deficiency caused by a novel ACAD9 mutation not responding to riboflavin treatment. *JIMD Rep.*, **12**, 37–45.
  55. Reyon, D., Tsai, S., Khayter, C., Foden, J., Sander, J. and Joung, J. (2012) FLASH assembly of TALENs for high-throughput genome editing. *Nat. Biotech.*, **30**, 460–465.
  56. McKenzie, M., Lazarou, M. and Ryan, M.T. (2009) Analysis of respiratory chain complex assembly with radiolabeled nuclear- and mitochondrial-encoded subunits. *Methods Enzymol.*, **456**, 321–339.
  57. Rappsilber, J., Mann, M. and Ishihama, Y. (2007) Protocol for micro-purification, enrichment, pre-fractionation and storage of peptides for proteomics using StageTips. *Nat. Protoc.*, **2**, 1896–1906.
  58. Cox, J. and Mann, M. (2008) MaxQuant enables high peptide identification rates, individualized p.p.b.-range mass accuracies and proteome-wide protein quantification. *Nat. Biotech.*, **26**, 1367–1372.
  59. Cox, J., Neuhauser, N., Michalski, A., Scheltema, R.A., Olsen, J.V. and Mann, M. (2011) Andromeda: a peptide search engine integrated into the MaxQuant environment. *J. Proteome Res.*, **10**, 1794–1805.
  60. Frazier, A.E. and Thorburn, D.R. (2012) Biochemical analyses of the electron transport chain complexes by spectrophotometry. *Methods Mol. Biol.*, **837**, 49–62.
  61. Schagger, H. and von Jagow, G. (1987) Tricine-sodium dodecyl sulfate-polyacrylamide gel electrophoresis for the separation of proteins in the range from 1 to 100 kDa. *Anal. Biochem.*, **166**, 368–379.
  62. Zerbetto, E., Vergani, L. and Dabbeni-Sala, F. (1997) Quantification of muscle mitochondrial oxidative phosphorylation enzymes via histochemical staining of blue native polyacrylamide gels. *Electrophoresis*, **18**, 2059–2064.

# Increased oxidative stress is related to disease severity in the ALS motor cortex

## A PET study

Masamichi Ikawa, MD,  
PhD  
Hidehiko Okazawa, MD,  
PhD  
Tetsuya Tsujikawa, MD,  
PhD  
Akiko Matsunaga, MD,  
PhD  
Osamu Yamamura, MD,  
PhD  
Tetsuya Mori, PhD  
Tadanori Hamano, MD,  
PhD  
Yasushi Kiyono, PhD  
Yasunari Nakamoto, MD,  
PhD  
Makoto Yoneda, MD,  
PhD

Correspondence to  
Dr. Yoneda:  
myoneda@fpu.ac.jp

### ABSTRACT

**Objective:** To investigate cerebral oxidative stress based on an over-reductive state caused by mitochondrial dysfunction and its relationship to disease severity in patients with amyotrophic lateral sclerosis (ALS) using PET with [<sup>62</sup>Cu]diacetyl-bis(N<sup>4</sup>-methylthiosemicarbazone) (<sup>62</sup>Cu-ATSM).

**Methods:** Twelve patients with ALS and 9 age-matched healthy controls underwent a 20-minute dynamic brain PET scan after <sup>62</sup>Cu-ATSM injection. The standardized uptake value (SUV) images obtained from the last 10 minutes of frames were normalized by the global mean (nSUV). Regional <sup>62</sup>Cu-ATSM retention in the nSUV images was compared between groups using statistical parametric mapping (SPM) and region of interest (ROI) analysis. Secondary analyses evaluated the correlations between regional nSUVs and the clinical characteristics of the participants.

**Results:** In SPM mapping, patients with ALS showed a significantly greater accumulation of <sup>62</sup>Cu-ATSM compared to controls in the bilateral cortices around the central sulcus, including the motor cortex, and the right superior parietal lobule. ROI analysis also revealed significantly greater nSUVs in patients than controls in these regions. Increases in nSUV for these regions were associated with decreases in the revised ALS Functional Rating Scale score, suggesting a good correlation with the severity of ALS. In controls, age was correlated with nSUV for the bilateral cortices around the central sulcus, although this correlation was not observed in patients with ALS.

**Conclusions:** <sup>62</sup>Cu-ATSM PET imaging demonstrated increased oxidative stress based on an over-reductive state, primarily in the motor cortex, in patients with ALS. The magnitude of oxidative stress correlated well with clinical severity, indicating that it may be associated with neurodegenerative changes in ALS. *Neurology*® 2015;84:2033-2039

### GLOSSARY

**ALS** = amyotrophic lateral sclerosis; **ALSFRS-R** = Revised Amyotrophic Lateral Sclerosis Functioning Rating Scale; **ANOVA** = analysis of variance; **MELAS** = mitochondrial myopathy, encephalopathy, lactic acidosis, and stroke-like episodes syndrome; **MNI** = Montreal Neurological Institute; **nSUV** = normalized standardized uptake value; **ROI** = region of interest; **ROS** = reactive oxygen species; **SUV** = standardized uptake value.

Amyotrophic lateral sclerosis (ALS) is characterized by the progressive degeneration of both upper and lower motor neurons.<sup>1</sup> Although the cause of the disease remains unknown in sporadic ALS without an apparent genetic component, increasing evidence from postmortem and biochemical investigations demonstrates that oxidative stress based on mitochondrial dysfunction is one of the principal molecular mechanisms for motor neuron degeneration in ALS.<sup>2,3</sup> However, the effects of oxidative stress on the neurodegeneration process in living patients with ALS remain to be elucidated. In addition, the clinical need for new diagnostic tools for ALS has been advocated.

Oxidative stress occurs upon increased production of reactive oxygen species (ROS), which are mostly generated by leakage of excess electrons from an over-reduction state in impaired mitochondrial respiratory chains,<sup>4,5</sup> suggesting that imaging of an over-reductive state would be

Supplemental data  
at [Neurology.org](http://Neurology.org)

From the Second Department of Internal Medicine, Faculty of Medical Sciences (M.I., A.M., O.Y., T.H., Y.N.), and Biomedical Imaging Research Center (H.O., T.T., T.M., Y.K., M.Y.), University of Fukui; and Faculty of Nursing and Social Welfare Sciences (M.Y.), Fukui Prefectural University, Japan.

Go to [Neurology.org](http://Neurology.org) for full disclosures. Funding information and disclosures deemed relevant by the authors, if any, are provided at the end of the article.

© 2015 American Academy of Neurology

2033

© 2015 American Academy of Neurology. Unauthorized reproduction of this article is prohibited.



a promising marker for oxidative stress. [<sup>62</sup>Cu]diacetyl-bis(*N*<sup>4</sup>-methylthiosemicarbazone) (<sup>62</sup>Cu-ATSM) is a PET radioligand for an intracellular over-reductive state.<sup>6-8</sup> Indeed, an increased retention of Cu-ATSM was observed in *in vitro* cell lines that were in an over-reductive state due to mitochondrial failure.<sup>7,8</sup> A large retention of <sup>62</sup>Cu-ATSM *in vivo* in the brains of patients with an inherited mitochondrial disorder or Parkinson disease also indicates the feasibility of this radioligand for the imaging of oxidative stress due to an over-reductive state.<sup>9,10</sup>

The aim of the current study was to evaluate cerebral oxidative stress and its relationship with the clinical features of patients with sporadic ALS using <sup>62</sup>Cu-ATSM PET to clarify the role of oxidative stress in the pathogenesis of ALS.

**METHODS Participants.** Twelve patients with sporadic ALS (7 men and 5 women) aged 65.2 ± 9.4 years who fulfilled the criteria of clinically probable or definite ALS according to the Revised El Escorial Diagnostic Criteria and who did not have obvious dementia were recruited at the University of Fukui Hospital, Japan (table). All patients presented with increased deep tendon reflexes or pathologic reflexes as well as muscle weakness and atrophy in more than 2 regions. Bulbar onset was seen in 2 patients. Eight of the patients showed a right-side dominant onset. The severity of their symptoms at the time of the scan was assessed using the Revised ALS Functioning Rating Scale (ALSFRS-R), which is graded from 48 (normal function) to 0, and the mean score was 30.9 ± 11.8. The mean disease duration was 25.8 ± 17.1 months. All patients with ALS were being treated with riluzole, but none of the patients was taking any

antioxidants such as vitamin C or vitamin E at the time of the PET evaluation. All patients with ALS underwent brain CT or MRI, and there was no apparent lesion or atrophy in the cerebral cortex. Nine age-matched healthy volunteers (6 men and 3 women) who were aged 61.2 ± 8.0 years were also recruited from a local community as normal controls. Seven controls were right-handed.

**Standard protocol approvals, registrations, and patient consents.** The protocol used for this study was approved by the Institutional Review Board of the University of Fukui. All participants provided written informed consent before participating in the study.

**PET procedure.** The detailed radioligand preparation and acquisition of <sup>62</sup>Cu-ATSM PET are described in appendix e-1 on the *Neurology*<sup>®</sup> Web site at Neurology.org. In brief, all participants underwent a 20-minute dynamic PET scan for the whole brain after an IV bolus injection of <sup>62</sup>Cu-ATSM. <sup>62</sup>Cu-ATSM was synthesized using a previously reported method.<sup>6,11</sup>

**Image data processing and analysis.** The reconstructed <sup>62</sup>Cu-ATSM images were converted into semiquantitative images in standardized uptake value (SUV) units. The SUV is the ratio of the decay-corrected activity per unit volume of tissue to the administered activity per unit of body weight. Early- and delayed-phase images were produced by averaging the dynamic PET data for the first 3 minutes and the last 10 minutes of frames, respectively.<sup>9,10,12</sup> Using Statistical Parametric Mapping 2 (SPM2; Wellcome Department of Cognitive Neurology, London, UK), individual delayed-phase SUV images were anatomically standardized using the individual parameters determined from the early-phase images and were transformed into Montreal Neurological Institute (MNI) space. A partial volume effect was not corrected. The spatially normalized dataset of images was then normalized by tissue activity (global mean = 100) after being smoothed with an 8-mm isotropic Gaussian filter. This facilitated comparisons of relative uptake across participants. Using this process, the SUV data from the delayed phase were normalized by the global mean (nSUV).

SPM2 was employed to identify regions with a significant increase in <sup>62</sup>Cu-ATSM retention in the ALS patient group compared to the control group in the nSUV image dataset. A voxel-wise correlation analysis of nSUV and ALSFRS-R scores in patients with ALS and of nSUV and age in controls was also performed. This processing used *t* statistics with the statistical threshold set at *p* < 0.01 at the voxel level and at *p* < 0.05 with a correction for multiple comparisons via the false discovery rate at the cluster level for the entire brain.

For each region where the SPM mapping showed a significant increase in retention in the ALS patient group, regions of interest (ROIs) were applied to the nSUV image of each participant. The regional nSUVs obtained were compared between the patients with ALS and controls, and their correlations with the demographic or clinical characteristics were assessed within each group. Time radioactivity curves were obtained from the regions where the SPM mapping showed significance and the pons. Average images were created for each group of nSUV images in the MNI space.

**Statistical analyses.** Data are given as the mean ± SD. All statistical analyses were performed using SPSS statistics version 17.0, and *p* < 0.05 was considered significant. A 2-tailed unpaired *t* test was used to evaluate differences in age between the groups. Categorical variables were compared across the groups using Fisher exact tests. Differences in the regional nSUV between and within participant groups were assessed using

Patient	Age, y	Sex	Disease duration, mo	ALSFRS-R score	Site of onset
1	43	F	18	41	R upper limb
2	68	M	17	41	L upper limb
3	68	F	72	11	R lower limb
4	63	M	48	43	R lower limb
5	73	F	24	13	L lower limb
6	80	M	24	30	B upper limb
7	66	M	17	40	Bulbar
8	69	F	24	39	R lower limb
9	61	M	20	18	R upper limb
10	55	M	13	41	R lower limb
11	64	F	17	25	L upper limb
12	72	M	16	29	Bulbar

Abbreviations: ALS = amyotrophic lateral sclerosis; ALSFRS-R = Revised Amyotrophic Lateral Sclerosis Functioning Rating Scale; B = bilateral. ALSFRS-R scores range from 48 (normal function) to 0.



analysis of variance (ANOVA) for repeated measures using post hoc Bonferroni correction, with diagnosis as a between-subjects factor and brain region as a within-subjects factor. Regression analysis between the regional nSUV and clinical characteristics within each group was performed using a Pearson rank correlation coefficient ( $r$ ).

**RESULTS** No significant differences were found in the age and sex distribution between the patients with ALS and the controls. There were no significant correlations among age, ALSFRS-R, and disease duration in patients with ALS.

Using SPM mapping, a significantly greater accumulation of  $^{62}\text{Cu}$ -ATSM in patients with ALS than in controls was observed, primarily in the bilateral cortices around the central sulcus, including the precentral and postcentral gyrus and paracentral lobule, as well as in the right superior parietal lobule (figure 1). The MNI coordinates of the peak uptake with the

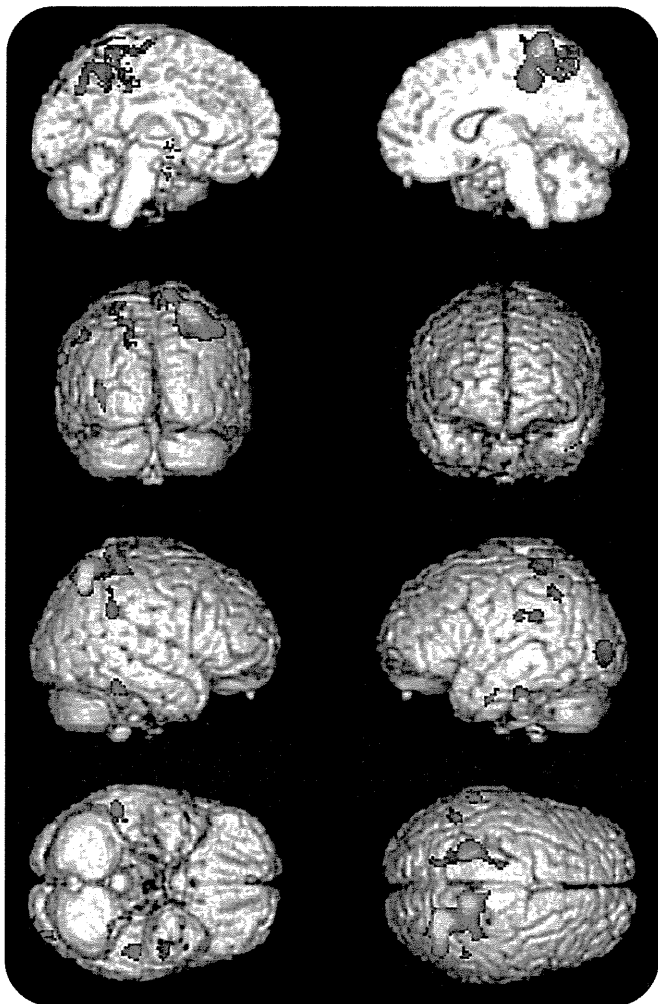
highest  $Z$  score in each significant cluster from SPM2 corresponded to the right paracentral lobule (10, -34, 46) and the left postcentral gyrus (-22, -42, 62). The average images of the delayed phase also show that  $^{62}\text{Cu}$ -ATSM retention in these regions of the ALS group was higher than that found in the controls (figure e-1). In addition, the time radioactivity curves of a representative patient with ALS showed the delayed-phase retention for the left cortex around the central sulcus was greater than that of pons, although those showed similar radioactivities in the early phase (figure e-2), suggesting that the delayed-phase retention is not affected by the early-phase uptake.

ANOVA analysis also revealed that the mean nSUV obtained by ROI analysis in patients with ALS was greater than that of controls in both the right and left cortices around the central sulcus and the right superior parietal lobule ( $p < 0.001$ , 0.005, and 0.001, respectively) (figure 2). Moreover, the average of the bilateral cortices around the central sulcus also showed a greater nSUV in the ALS group than in the controls ( $p < 0.001$ ). The mean nSUV in the left cortex around the central sulcus was greater than that in the right cortex around the central sulcus in both groups (both  $p < 0.001$ ).

Figure 3 shows the correlations between the ALSFRS-R score and each nSUV for the right, left, and bilateral cortices around the central sulcus and for the right superior parietal lobule in patients with ALS. The nSUV for all target regions had a linear correlation with the ALSFRS-R score ( $r = -0.64$ ,  $-0.58$ ,  $-0.69$ , and  $-0.62$ , respectively;  $p < 0.05$  for all correlations), suggesting that the retention in these regions increased with the clinical severity of ALS. There were no significant correlations between any nSUVs for these regions and disease duration in patients with ALS. Although there was also no significant correlation between age and any nSUV in patients with ALS, age was correlated with both nSUVs for the right and bilateral cortices around the central sulcus in controls ( $r = 0.72$  and  $0.76$ , respectively;  $p < 0.05$  for both correlations) (figure 4). A voxel-wise correlation analysis showed no significant correlations between the nSUV and ALSFRS-R score in patients with ALS or between the nSUV and age in the controls, most likely due to the small number of participants and no partial-volume correction.

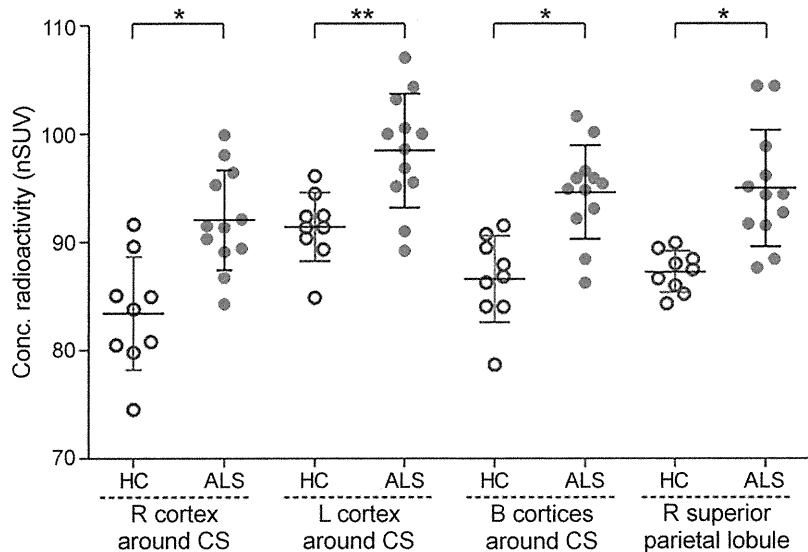
**DISCUSSION** In this study, we found greater  $^{62}\text{Cu}$ -ATSM retention in patients with ALS than in controls within bilateral cortical regions, including the motor cortex, as well as in the right superior parietal lobule (figures 1 and 2). Because the primary motor cortex is included not only in the precentral gyrus but also in the postcentral gyrus and the

**Figure 1** Greater retention of  $^{62}\text{Cu}$ -ATSM in patients with amyotrophic lateral sclerosis (ALS) than healthy controls in statistical parametric mapping (SPM) analysis



SPM results display the regions in which  $^{62}\text{Cu}$ -ATSM retention was higher in patients with ALS than in healthy controls (voxel-level threshold was  $p < 0.01$ ).

**Figure 2 Comparisons of regional  $^{62}\text{Cu}$ -ATSM retention between patients with amyotrophic lateral sclerosis (ALS) and healthy controls (HC)**



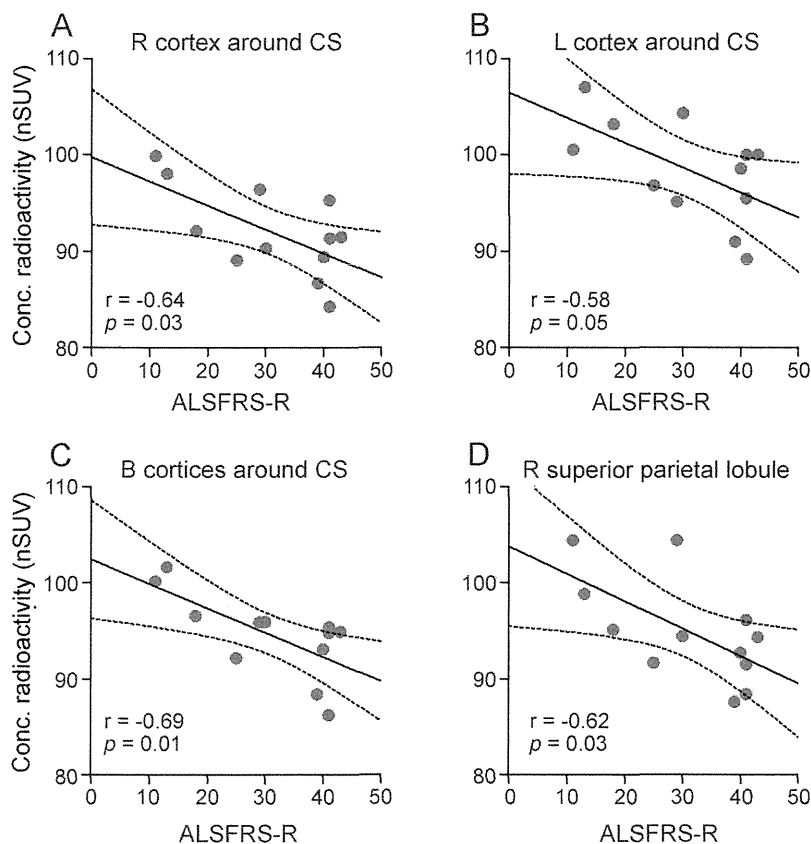
Standardized uptake values of  $^{62}\text{Cu}$ -ATSM normalized by the global mean (nSUV) are greater in patients with ALS than HC in the right, left, and bilateral (B) cortex around the central sulcus (CS), as well as the right superior parietal lobule. Data are presented as the mean  $\pm$  SD. Significant at \* $p < 0.001$  and \*\* $p < 0.005$ .

paracentral lobule,<sup>13,14</sup> most of the regions showing high uptake around the central sulcus may correspond to the motor cortex. Increased retention in the superior parietal lobule may also be associated with the high retention in motor cortex because there are tight cortical connections between the motor areas and the motor-related parietal areas.<sup>15,16</sup> Moreover, the tracer retention in these regions increased with the clinical severity, as estimated by the ALSFRS-R score, in patients with ALS (figure 3). Studies using cell lines with mitochondrial respiratory failure have demonstrated that high levels of Cu-ATSM retention indicate an over-reductive state that would lead to oxidative stress.<sup>7,8</sup> Therefore, the correlation between increased  $^{62}\text{Cu}$ -ATSM retention and disease severity in both the motor cortex and motor-related parietal cortex of patients with ALS suggests the presence of enhanced oxidative stress based on mitochondrial dysfunction in the ALS brain and points to its contribution to the motoneuronal degenerative progression in ALS.

In vivo imaging of oxidative stress based on mitochondrial dysfunction has been strongly required in ALS because of a number of studies indicating that oxidative stress and mitochondrial dysfunction play a major role in motor neuron degeneration in ALS.<sup>2,3</sup> Increases in the levels of 8-hydroxy-2'-deoxyguanosine (8-OHdG), protein carbonyls, or 4-hydroxy-2-nonenal (4-HNE) histidine in the motor cortex or spinal cord in patients with ALS compared to healthy controls have been demonstrated in

multiple postmortem studies,<sup>17–20</sup> indicating the accumulation of oxidative damage to DNA, proteins, and lipids in ALS. Increased concentrations of 8-OHdG or 4-HNE in the blood, urine, and CSF of patients with ALS compared to those of healthy participants have also been found in recent studies.<sup>21–23</sup> In addition, these studies showed that serum 4-HNE or urine 8-OHdG levels correlated with advancing disease or clinical severity, as indicated by the ALSFRS-R score, in patients with ALS.<sup>21,23</sup> These findings, which are consistent with our study, suggest that oxidative stress increases with disease progression in ALS. Similarly, abnormalities of mitochondria and mitochondrial respiratory failure have been identified in sporadic human ALS.<sup>3</sup> Transgenic mice and cell culture models carrying mutant Cu/Zn superoxide dismutase (*SOD1*) gene also showed mitochondrial abnormalities.<sup>24</sup> However, these pathologic or biochemical studies cannot dynamically identify regional changes of oxidant status or mitochondrial function in living patients.  $^{62}\text{Cu}$ -ATSM PET imaging can be a promising biomarker for evaluating regional oxidative stress, based on an over-reductive state caused by mitochondrial dysfunction in the brains of patients with ALS, because this radioligand is retained in sites with an over-reductive state in the delayed phase after injection due to the reduction of Cu(II) in Cu-ATSM.<sup>6–8</sup> An over-reductive state is the state in which cells and tissues have excessive levels of electrons relative to  $\text{O}_2$ , which is caused by impaired respiratory chains or hypoxia, and oxidative stress is induced by excess ROS produced from redundant electrons in this state under mitochondrial dysfunction.<sup>4,5,7–10</sup> In fact, increased retention of Cu-ATSM correlated with the levels of the biological reductants NADH and NADPH was observed in cell lines with an over-reductive state caused by mutated mitochondria.<sup>7,8</sup> Furthermore, in living patients, we found an increased retention of  $^{62}\text{Cu}$ -ATSM in brain lesions due to mitochondrial myopathy, encephalopathy, lactic acidosis, and stroke-like episodes syndrome (MELAS), the most common mitochondrial disease due to a known mutation in mitochondrial DNA,<sup>9</sup> and in the striatum in Parkinson disease.<sup>10</sup> Mitochondrial dysfunction and oxidative damage have been demonstrated pathologically and biochemically in the postmortem brains of individuals with these diseases.<sup>25,26</sup> On the other hand, this radioligand readily crosses the blood–brain barrier with a high membrane permeability in the early phase after injection,<sup>6</sup> indicating that the early-phase uptake reflects the cerebral blood flow.<sup>9,12</sup> The time radioactivity curves in the present study and our previous PET studies showed that the regional blood flow indicated by the early-phase uptake is not related to the retention in the delayed phase unless the region is not hyporemic

**Figure 3 Relationships between  $^{62}\text{Cu}$ -ATSM retention and Revised Amyotrophic Lateral Sclerosis Functioning Rating Scale (ALSFRS-R) score in patients with amyotrophic lateral sclerosis (ALS)**



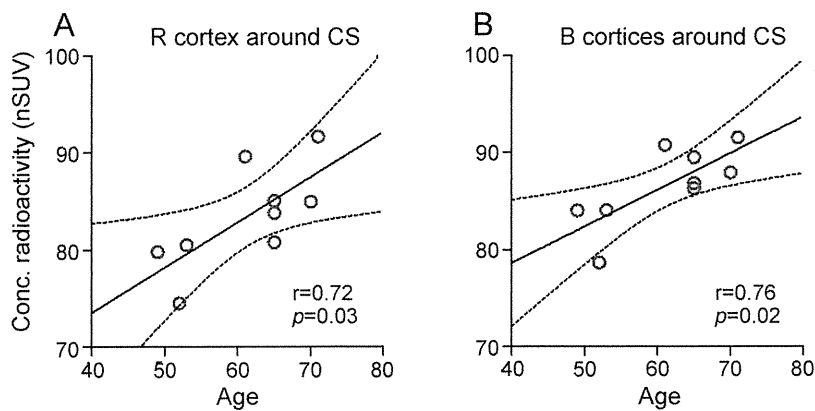
ALS participants: regression analyses between ALSFRS-R score and each standardized uptake value of  $^{62}\text{Cu}$ -ATSM, normalized by the global mean (nSUV), in the right (A), left (B), and bilateral (B) (C) cortex around the central sulcus (CS), as well as the right superior parietal lobule (D). Pearson coefficients ( $r$ ) and  $p$  values are shown for each relationship. ALSFRS-R scores range from 48 (normal function) to 0.

(figure e-2).<sup>9,10</sup> Although  $^{62}\text{Cu}$ -ATSM nonspecifically binds to serum proteins,<sup>27,28</sup> which can impact the early-phase uptake due to the blood flow, the delayed-phase retention may be less affected by this nonspecific binding because the lipophilicity of this radioligand decreases within 15 minutes, indicating that the metabolites may not enter the brain in the delayed phase.<sup>28</sup> Taken together, both in vitro and in vivo studies demonstrated the selectivity of  $^{62}\text{Cu}$ -ATSM retention for an over-reductive state, suggesting that  $^{62}\text{Cu}$ -ATSM PET can selectively detect oxidative stress based on this state in patients with neurodegenerative disorders associated with oxidative injury and mitochondrial failure, including ALS. Interestingly, the therapeutic potential of non-radiolabeled Cu-ATSM was shown in ALS model mice.<sup>29-31</sup> Cu-ATSM has a potential to detoxify mutant SOD1 by supplying Cu to Cu-deficient mutant SOD1 as well as antioxidant activity, also indicating the high selectivity of Cu-ATSM for the disease-affected tissues in ALS.

Other mechanisms involved in the pathophysiology of sporadic ALS, such as neuroinflammation caused mainly by activated microglia, may be associated with oxidative stress based on an over-reductive state in ALS because inflammatory cells induce ROS generation and increased ROS stimulate activation of these cells.<sup>32,33</sup> A recent PET study using  $^{18}\text{F}$ -DPA-714, a radioligand for the 18 kDa translocator protein (TSPO) expressed on cerebral inflammatory cells, showed enhanced neuroinflammation in several cortical regions including the primary motor, supplementary motor, and temporal cortices of patients with sporadic ALS at an early stage of the disease.<sup>34</sup> This finding and our results suggest that oxidative stress and neuroinflammation may occur concurrently and induce neurodegeneration in the brains of patients with ALS. Similarly, changes of glucose metabolism may also be related to oxidative stress due to mitochondrial dysfunction because glycolytic hypermetabolism can produce abundant NADH burdening excess electrons to the impaired respiratory chains.<sup>9,35</sup> However, the regions of relatively increased  $^{62}\text{Cu}$ -ATSM retention in ALS in the present study were not consistent with the regions where recent  $^{18}\text{F}$ -fludeoxyglucose ( $^{18}\text{F}$ -FDG) PET studies showed increased metabolism, which were mainly the brainstem and medial temporal cortex.<sup>36,37</sup> Our previous PET study demonstrated that increased uptake of  $^{18}\text{F}$ -FDG precedes elevated retention of  $^{62}\text{Cu}$ -ATSM in the brain lesions of MELAS,<sup>9</sup> suggesting that a period of hypermetabolism may be inconsistent with that of oxidative stress under mitochondrial dysfunction. The relationship between these mechanisms should be elucidated by future studies.

In this study,  $^{62}\text{Cu}$ -ATSM retention in the right and bilateral cortices around the central sulcus increased with age only in healthy controls but not in patients with ALS (figure 4). Recent reports also showed correlations between age and concentrations of 8-OHdG in the urine, plasma, and CSF combining patients with ALS and healthy controls,<sup>21,22</sup> suggesting that oxidative stress is associated with normal aging in healthy individuals as well as with disease progression in patients with ALS. In addition, the higher retention in left cortex around the central sulcus than the right cortex in both patients with ALS and controls was also shown in the present study (figure 2). The higher retention in the left cortex may be associated with the laterality of symptoms at the onset in patients or the handedness side in controls because of the right-side-dominant onset in most patients and the right-handedness in most controls. Construction of a database for healthy humans would be helpful to validate the relationship between the regional retention and aging or handedness.

Figure 4 Relationships between  $^{62}\text{Cu}$ -ATSM retention and age in healthy controls



Healthy control participants: regression analyses between age and each standardized uptake value of  $^{62}\text{Cu}$ -ATSM, normalized by the global mean (nSUV), in the right (A) and bilateral (B) cortex around the central sulcus (CS). Pearson coefficients ( $r$ ) and  $p$  values are shown for each relationship.

### Comment: Cu-ATSM to treat and image amyotrophic lateral sclerosis

Diagnostic imaging for amyotrophic lateral sclerosis (ALS) has the potential to alleviate elements of uncertainty associated with the current diagnostic process and to improve probability of successful outcomes from therapeutic clinical trials via earlier enrollment and treatment of participants. Ikawa et al.<sup>1</sup> describe outcomes from an assessment of  $^{62}\text{Cu}$ -ATSM in patients with ALS using PET. Selective accumulation of the radiotracer in the motor cortex of patients with ALS and its correlation with disease severity supports the use of this compound to image ALS via PET. Although the study involved a limited number of participants (12 ALS and 9 healthy controls), the outcomes are nonetheless encouraging. Increasing radioactive half-life of the tracer by using  $^{64}\text{Cu}$ -ATSM (12 hours) instead of  $^{62}\text{Cu}$ -ATSM (10 minutes) together with a longer postinjection imaging interval could afford greater sensitivity and thereby better insight to whether Cu-ATSM PET may be used for diagnostic purposes.

In addition to the present ALS study, Ikawa et al.<sup>2</sup> have previously demonstrated the potential to use Cu-ATSM PET to image Parkinson disease (PD). Herein lies a tantalizing prospect: Therapeutic testing of Cu-ATSM in rodent models of ALS and PD has generated robust positive outcomes, including neuroprotection in the primary site of pathology as well as improved locomotive and cognitive function of the animals.<sup>3,4</sup> It therefore appears that the potential imaging application of Cu-ATSM in ALS and PD is matched by its potential as a therapeutic. Whether or not the imaging and therapeutic activities of Cu-ATSM in these 2 neurodegenerative diseases are related at a cellular mechanism of action level remains to be elucidated.

1. Ikawa M, Okazawa H, Tsujikawa T, et al. Increased oxidative stress is related to disease severity in the ALS motor cortex: a PET study. *Neurology* 2015;84:2033–2039.
2. Ikawa M, Okazawa H, Kudo T, et al. Evaluation of striatal oxidative stress in patients with Parkinson's disease using [ $^{62}\text{Cu}$ ]ATSM PET. *Nucl Med Biol* 2011;38:945–951.
3. Roberts BR, Lim NK, McAllum EJ, et al. Oral treatment with Cu<sup>II</sup>(ATSM) increases mutant SOD1 *in vivo* but protects motor neurons and improves the phenotype of a transgenic mouse model of amyotrophic lateral sclerosis. *J Neurosci* 2014;34:8021–8031.
4. Hung LW, Villemagne VL, Cheng L, et al. The hypoxia imaging agent Cu<sup>II</sup>(ATSM) is neuroprotective and improves motor and cognitive functions in multiple animal models of Parkinson's disease. *J Exp Med* 2012;209:837–854.

Peter J. Crouch, PhD

From the Department of Pathology and Florey Institute of Neuroscience and Mental Health, The University of Melbourne, Victoria, Australia.

Study funding: No targeted funding reported.

Disclosure: P.J. Crouch is an employee of The University of Melbourne. Collaborative Medicinal Development LLC has licensed intellectual property on this subject from The University of Melbourne. Dr. Crouch receives/has received research support from the National Health and Medical Research Council, the Motor Neurone Disease Research Institute of Australia, The CASS Foundation, Bethlehem Griffiths Research Foundation, ANZ Charitable Trusts, and The University of Melbourne. Go to [Neurology.org](http://Neurology.org) for full disclosures.

The limitations of this study include the small number of participants and the overlaps in the degree (nSUV) of regional  $^{62}\text{Cu}$ -ATSM retention between the ALS and control groups (figure 2). Although the results clearly demonstrate underlying oxidative stress in patients with ALS, this method remains impractical for clinical diagnostic purposes. Further studies utilizing a large number of participants are necessary to confirm our preliminary results. In addition,  $^{64}\text{Cu}$ -ATSM, which has a longer half-life than  $^{62}\text{Cu}$ -ATSM, may improve the signal-to-noise ratio and increase detection power for oxidative stress associated with an over-reductive state in future PET studies.<sup>7,31</sup>

We have shown that  $^{62}\text{Cu}$ -ATSM PET can non-invasively provide information on cerebral oxidative stress due to an over-reductive state in patients with ALS. Increased oxidative stress in motor and motor-related cortices correlated strongly with disease severity, suggesting that oxidative stress is associated with neurodegeneration in ALS. PET imaging with  $^{62}\text{Cu}$ -ATSM for oxidative stress based on mitochondrial dysfunction may improve our insights into the pathogenesis of ALS and may be a promising tool for monitoring further antioxidant and mitochondrial therapies.

### AUTHOR CONTRIBUTIONS

Dr. Ikawa: design and conceptualization of the study, analysis and interpretation of the data, acquisition of data, statistical analysis, drafting and revising the manuscript for intellectual content. Prof. Okazawa: design and conceptualization of the study, analysis and interpretation of data, acquisition of data, statistical analysis, drafting and revising the manuscript for intellectual content, study supervision and coordination. Dr. Tsujikawa: analysis and interpretation of the data, acquisition of data. Dr. Matsunaga: analysis and interpretation of the data, acquisition of data. Dr. Yamamura: analysis and interpretation of the data, acquisition of data. Dr. Mori: analysis and interpretation of the data, acquisition of data. Dr. Hamano: analysis and interpretation of the data, acquisition of data. Prof. Kiyono: analysis and interpretation of the data, acquisition of data, study coordination. Prof. Nakamoto: revising the manuscript for intellectual content, study supervision. Prof. Yoneda: design and conceptualization of the study, analysis and interpretation of data, acquisition of data, revising the manuscript for intellectual content, study supervision and coordination.

### STUDY FUNDING

Supported in part by Grants-in-Aid for Scientific Research on Innovative Areas (24111517) and Scientific Research (C) (25461311) from the Japan Society for the Promotion of Science.

### DISCLOSURE

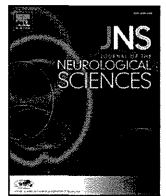
The authors report no disclosures relevant to the manuscript. Go to [Neurology.org](http://Neurology.org) for full disclosures.

Received August 15, 2014. Accepted in final form January 15, 2015.

### REFERENCES

1. Rowland LP, Shneider NA. Amyotrophic lateral sclerosis. *N Engl J Med* 2001;344:1688–1700.
2. D'Amico E, Factor-Litvak P, Santella RM, Mitsumoto H. Clinical perspective on oxidative stress in sporadic amyotrophic lateral sclerosis. *Free Radic Biol Med* 2013;65:509–527.

3. Manfredi G, Xu Z. Mitochondrial dysfunction and its role in motor neuron degeneration in ALS. *Mitochondrion* 2005;5:77–87.
4. Lenaz G, Bovina C, D'Aurelio M, et al. Role of mitochondria in oxidative stress and aging. *Ann NY Acad Sci* 2002; 959:199–213.
5. Indo HP, Davidson M, Yen HC, et al. Evidence of ROS generation by mitochondria in cells with impaired electron transport chain and mitochondrial DNA damage. *Mitochondrion* 2007;7:106–118.
6. Fujibayashi Y, Taniuchi H, Yonekura Y, Ohtani H, Konishi J, Yokoyama A. Copper-62-ATSM: a new hypoxia imaging agent with high membrane permeability and low redox potential. *J Nucl Med* 1997;38: 1155–1160.
7. Yoshii Y, Yoneda M, Ikawa M, et al. Radiolabeled Cu-ATSM as a novel indicator of overreduced intracellular state due to mitochondrial dysfunction: studies with mitochondrial DNA-less  $\rho^0$  cells and cybrids carrying MELAS mitochondrial DNA mutation. *Nucl Med Biol* 2012;39: 177–185.
8. Donnelly PS, Liddell JR, Lim S, et al. An impaired mitochondrial electron transport chain increases retention of the hypoxia imaging agent diacetylbis (4-methylthiosemicarbazonato) copper II. *Proc Natl Acad Sci USA* 2012;109:47–52.
9. Ikawa M, Okazawa H, Arakawa K, et al. PET imaging of redox and energy states in stroke-like episodes of MELAS. *Mitochondrion* 2009;9:144–148.
10. Ikawa M, Okazawa H, Kudo T, Kuriyama M, Fujibayashi Y, Yoneda M. Evaluation of striatal oxidative stress in patients with Parkinson's disease using [ $^{62}\text{Cu}$ ] ATSM PET. *Nucl Med Biol* 2011;38:945–951.
11. Lohith TG, Kudo T, Demura Y, et al. Pathophysiological correlation between  $^{62}\text{Cu}$ -ATSM and  $^{18}\text{F}$ -FDG in lung cancer. *J Nucl Med* 2009;50:1948–1953.
12. Isozaki M, Kiyono Y, Arai Y, et al. Feasibility of  $^{62}\text{Cu}$ -ATSM PET for evaluation of brain ischaemia and misery perfusion in patients with cerebrovascular disease. *Eur J Nucl Med Mol Imaging* 2011;38:1075–1082.
13. Penfield W, Boldrey E. Somatic motor and sensory representation in the cerebral cortex of man as studied by electrical stimulation. *Brain* 1937;60:389–443.
14. Kushchayev SV, Moskalenko VF, Wiener PC, et al. The discovery of the pyramidal neurons: Vladimir Betz and a new era of neuroscience. *Brain* 2012;135:285–300.
15. Rizzolatti G, Luppino G. The cortical motor system. *Neuron* 2001;31:889–901.
16. Cosottini M, Pesaresi I, Piazza S, et al. Magnetization transfer imaging demonstrates a distributed pattern of microstructural changes of the cerebral cortex in amyotrophic lateral sclerosis. *Am J Neuroradiol* 2011;32: 704–708.
17. Fitzmaurice PS, Shaw IC, Kleiner HE, et al. Evidence for DNA damage in amyotrophic lateral sclerosis. *Muscle Nerve* 1996;19:797–798.
18. Shaw PJ, Ince PG, Falkous G, Mantle D. Oxidative damage to protein in sporadic motor neuron disease spinal cord. *Ann Neurol* 1995;38:691–695.
19. Ferrante RJ, Browne SE, Shinobu LA, et al. Evidence of increased oxidative damage in both sporadic and familial amyotrophic lateral sclerosis. *J Neurochem* 1997;69: 2064–2074.
20. Shibata N, Nagai R, Uchida K, et al. Morphological evidence for lipid peroxidation and protein glycooxidation in spinal cords from sporadic amyotrophic lateral sclerosis patients. *Brain Res* 2001;917:97–104.
21. Bogdanov M, Brown RH, Matson W, et al. Increased oxidative damage to DNA in ALS patients. *Free Radic Biol Med* 2000;29:652–658.
22. Mitsumoto H, Santella RM, Liu X, et al. Oxidative stress biomarkers in sporadic ALS. *Amyotroph Lateral Scler* 2008;9:177–183.
23. Simpson EP, Henry YK, Henkel JS, Smith RG, Appel SH. Increased lipid peroxidation in sera of ALS patients: a potential biomarker of disease burden. *Neurology* 2004; 62:1758–1765.
24. Muyderman H, Chen T. Mitochondrial dysfunction in amyotrophic lateral sclerosis: a valid pharmacological target? *Br J Pharmacol* 2014;171:2191–2205.
25. Dexter DT, Carter CJ, Wells FR, et al. Basal lipid peroxidation in substantia nigra is increased in Parkinson's disease. *J Neurochem* 1989;52:381–389.
26. Katayama Y, Maeda K, Iizuka T, et al. Accumulation of oxidative stress around the stroke-like lesions of MELAS patients. *Mitochondrion* 2009;9:306–313.
27. Basken NE, Green MA. Cu(II) bis(thiosemicarbazone) radiopharmaceutical binding to serum albumin: further definition of species dependence and associated substituent effects. *Nucl Med Biol* 2009;36:495–504.
28. Hueting R, Kersemans V, Cornelissen B, et al. A comparison of the behavior of  $^{64}\text{Cu}$ -acetate and  $^{64}\text{Cu}$ -ATSM in vitro and in vivo. *J Nucl Med* 2014;55:128–134.
29. Soon CP, Donnelly PS, Turner BJ, et al. Diacetylbis (N(4)-methylthiosemicarbazonato) copper(II) (CuII(at-sm)) protects against peroxynitrite-induced nitrosative damage and prolongs survival in amyotrophic lateral sclerosis mouse model. *J Biol Chem* 2011;286:44035–44044.
30. McAllum EJ, Lim NK, Hickey JL, et al. Therapeutic effects of Cu(II)(at-sm) in the SOD1-G37R mouse model of amyotrophic lateral sclerosis. *Amyotroph Lateral Scler Frontotemporal Degener* 2013;14:586–590.
31. Roberts BR, Lim NK, McAllum EJ, et al. Oral treatment with Cu(II)(at-sm) increases mutant SOD1 in vivo but protects motor neurons and improves the phenotype of a transgenic mouse model of amyotrophic lateral sclerosis. *J Neurosci* 2014;34:8021–8031.
32. Kiernan MC, Vucic S, Cheah BC, et al. Amyotrophic lateral sclerosis. *Lancet* 2011;377:942–955.
33. Mhatre M, Floyd RA, Hensley K. Oxidative stress and neuroinflammation in Alzheimer's disease and amyotrophic lateral sclerosis: common links and potential therapeutic targets. *J Alzheimers Dis* 2004;6:147–157.
34. Corcia P, Tauber C, Vercoullie J, et al. Molecular imaging of microglial activation in amyotrophic lateral sclerosis. *PLoS One* 2012;7:e52941.
35. Ikawa M, Yoneda M, Tanaka M. Energy states in mitochondrial cardiomyopathy: in vivo functional imaging and L-arginine therapy. *Circ J* 2010;74:2560–2561.
36. Pagani M, Chiò A, Valentini MC, et al. Functional pattern of brain FDG-PET in amyotrophic lateral sclerosis. *Neurology* 2014;83:1067–1074.
37. Van Laere K, Vanhee A, Verschueren J, et al. Value of  $^{18}\text{F}$ fluorodeoxyglucose-positron-emission tomography in amyotrophic lateral sclerosis: a prospective study. *JAMA Neurol* 2014;71:553–561.



## FDG-PET study of patients with Leigh syndrome

Kauzhiro Haginoya<sup>a,b,\*</sup>, Tomohiro Kaneta<sup>c</sup>, Noriko Togashi<sup>d</sup>, Naomi Hino-Fukuyo<sup>a</sup>, Tomoko Kobayashi<sup>a</sup>, Mitsugu Uematsu<sup>a</sup>, Taro Kitamura<sup>e</sup>, Takehiko Inui<sup>b</sup>, Yukimune Okubo<sup>a,b</sup>, Yusuke Takezawa<sup>a,b</sup>, Mai Anzai<sup>b</sup>, Wakaba Endo<sup>a,b</sup>, Noriko Miyake<sup>f</sup>, Hirotomo Saito<sup>f</sup>, Naomichi Matsumoto<sup>f</sup>, Shigeo Kure<sup>a</sup>

<sup>a</sup> Department of Pediatrics, Tohoku University School of Medicine, Sendai 980-8574, Japan

<sup>b</sup> Department of Pediatric Neurology, Takuto Rehabilitation Center for Children, Sendai 982-0241, Japan

<sup>c</sup> Department of Radiology, Tohoku University School of Medicine, Sendai 980-8574, Japan

<sup>d</sup> Department of Neurology, Miyagi Children's Hospital, Sendai 989-3126, Japan

<sup>e</sup> Department of Pediatrics, Sendai City Hospital, Sendai 982-8502, Japan

<sup>f</sup> Department of Human Genetics, Yokohama City University Graduate School of Medicine, Yokohama 236-0004, Japan

### ARTICLE INFO

#### Article history:

Received 8 May 2015

Received in revised form 1 February 2016

Accepted 3 February 2016

Available online 4 February 2016

#### Keywords:

FDG-PET

Leigh syndrome

neuroimaging

positron emission tomography

mitochondrial disease

PET

### ABSTRACT

We conducted a [<sup>18</sup>F]fluorodeoxyglucose positron emission tomography (FDG-PET) study in five patients (median age 11 (range 4–13) years) with Leigh syndrome to evaluate its usefulness for understanding the functional brain dysfunction in this disease and in future drug trials. Four patients were found to have reported mitochondrial DNA gene mutations. The brain T2-weighted magnetic resonance imaging (MRI) showed high-intensity areas in the putamen bilaterally in five patients, caudate bilaterally in four, thalamus bilaterally in two, and brainstem in one. Cerebellar atrophy was observed in older two patients. For disease control, seven age-matched epilepsy patients who had normal MRI and FDG-PET studies were selected. For semiquantitative analysis of the lesions with decreased <sup>18</sup>F-FDG uptake, the mean standard uptake value (SUV) was calculated in regions of interest (ROIs) placed in each brain structure. We compared the SUV of nine segments (the frontal, temporal, parietal, and occipital lobes, thalami, basal ganglia, mid-brain, pons, and cerebellum) between patients with Leigh syndrome and controls. The glucose uptake was decreased significantly in the cerebellum and basal ganglia, which could explain the ataxia and dystonia in patients with Leigh syndrome. Although this study had some limitations, FDG-PET might be useful for evaluating the brain dysfunction and treatment efficacy of new drugs in patients with Leigh syndrome. Further study with more patients using advanced methods to quantify glucose uptake is needed before drawing a conclusion.

© 2016 Elsevier B.V. All rights reserved.

### 1. Introduction

Leigh syndrome is one of the most common mitochondrial disorders in children. An estimated pre-school incidence in western Sweden is 1 per 34,000 births [1]. It is characterized by neuropathological findings that include bilateral symmetrical lesions in the basal ganglia, thalamus, and brainstem [2–4]. These lesions appear hypodense on computed tomography and show hyperintense signal on T2-weighted and hypointense signal on T1-weighted magnetic resonance imaging (MRI) [2–4]. A comprehensive multicenter study showed that the median age of disease onset is 7 months [5]. The most common clinical features are abnormal motor findings such as hypotonia, dystonia,

spasticity and ataxia, followed by abnormal ocular findings, feeding difficulties, epileptic seizures, respiratory dysfunction and mental retardation [5]. Increased level of lactate in the cerebrospinal fluid is significantly correlated to a more severe disease course [5]. 39% of patients had died by the age of 21 years, at a median age of 2.4 years [5]. Recent advances in genetic research have shown that this devastating disorder is caused by mitochondrial and nuclear DNA mutations [5]. Nevertheless, the genetic cause remains unidentified in 40% of patients, in whom discovery of the cause is left for future whole exome sequencing studies [5].

Changes in the basal ganglia, thalamus, and brainstem detected using MRI have long been thought of as one of landmarks for a clinical diagnosis of Leigh syndrome [4], while the role of functional neuroimaging, including single photon emission computed tomography (SPECT) and positron emission tomography (PET), is not clear in patients with Leigh syndrome [6–9]. Hexamethylpropylene amine oxime (HMPAO)-SPECT showed decreased brain perfusion, especially in the cerebellum

\* Corresponding author at: Department of Pediatric Neurology, Takuto Rehabilitation Center for Children, 20 Shishio, Akiu Yumoto, Taihakoku, Sendai 982-0241, Japan.

E-mail address: [khaginoya@kha.biglobe.ne.jp](mailto:khaginoya@kha.biglobe.ne.jp) (K. Haginoya).

**Table 1**  
Clinical summary and results of gene analysis of five patients with Leigh syndrome

Patient no.	Sex	Onset	Age at FDG-PET	Initial symptoms	Gene analysis	Clinical symptoms at FDG-PET study	MRI findings at FDG-PET study	FDG-PET findings	Drugs at FDG-PET study
1	M	1 y	4 y	Tremor	Not done	Intellectual disability, truncal ataxia, tremor	Nodular high intensity lesions in the bilateral caudate, putamina and thalami on T2WI	Decreased metabolism in bilateral thalami, basal ganglia, temporal lobes and cerebellum	Vitamin B1, biotin, levodopa/carbidopa
2	M	6 y	7 y	Ophthalmoplegia, ptosis, squint	m. T10191C	Epilepsy, ophthalmoplegia, ataxic gait, intellectual disability	Punctate and sparse high intensity lesions in the bilateral putamina and thalami on T2WI, diffuse high intensity lesion in the mid brain on T2WI	Decreased metabolism in bilateral basal ganglia	Vitamin B1, biotin, anticonvulsants, levodopa/carbidopa
3	M	3 y	11 y	Ataxic-dystonic gait	m. T14887C	Intellectual disability, truncal ataxia, dystonia, ptosis, ophthalmoplegia, slurred speech	Diffuse high intensity lesions in the bilateral caudate and putamina on T2WI	Decreased metabolism in bilateral basal ganglia, thalami, temporal lobes and mid brain	Vitamin B1, biotin, coenzyme Q, dichloroacetate
4	F	1.5 y	12 y	Developmental delay	m. T8993G	Intellectual disability, truncal ataxia, ophthalmoplegia, slurred speech, bed ridden at febrile disorder	Diffuse high intensity lesions in the bilateral caudate and putamina on T2WI, cerebellar atrophy	Decreased metabolism in bilateral basal ganglia, thalami, temporal lobes and cerebellum	Vitamin B1, vitamin C, coenzyme Q, vitamin B12
5	M	2 y	13 y	Ataxic gait	m. T8993G	Intellectual disability, truncal ataxia, dystonia, spasticity of the legs, hyperactivity, regression with febrile disorder	Punctate high intensity lesions in the bilateral caudate and putamina on T2WI, cerebellar atrophy	Decreased metabolism in left frontal lobe, bilateral basal ganglia and cerebellum	Vitamin B1, vitamin C, biotin, coenzyme Q, arginine

and other structures[7–9]. [ $^{18}\text{F}$ ]fluorodeoxyglucose positron emission tomography (FDG-PET) performed in one patient showed decreased glucose uptake in the putamen and caudate [6]. A recent study used HMPAO-SPECT to evaluate new therapeutic agents for mitochondrial

disease, including Leigh syndrome [8–9]. We studied five patients with Leigh syndrome using FDG-PET to evaluate its usefulness for understanding the functional brain dysfunction in this disease and in future drug trials.

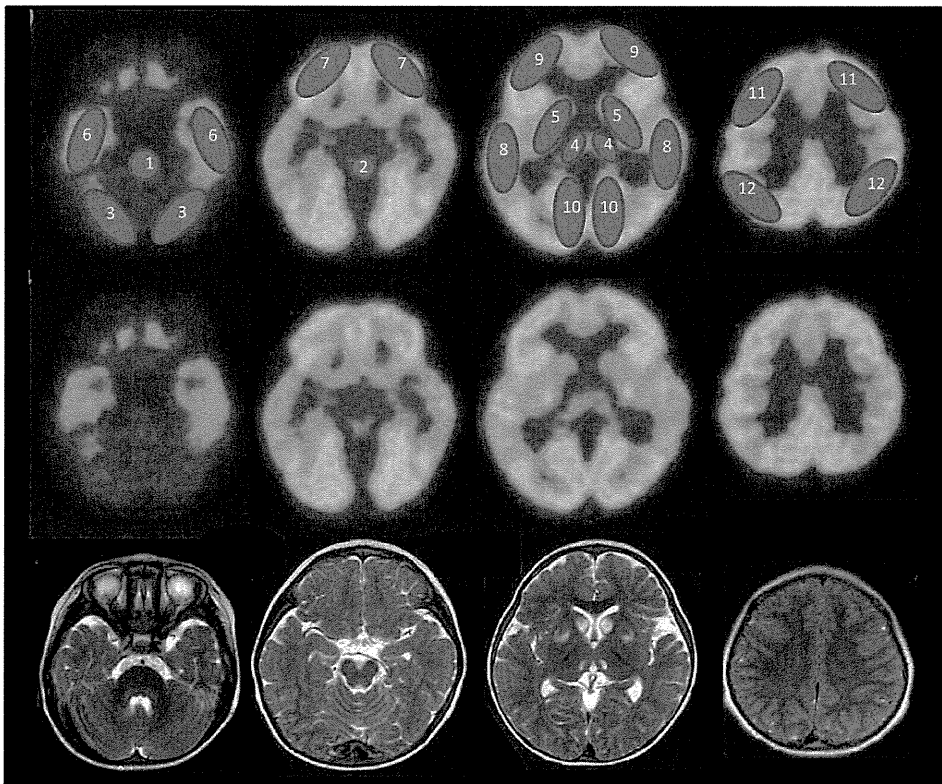


**Fig. 1.** Layout of the ROIs and the brain MRI (T2WI) in patient 1. ROIs were placed manually in the pons (1), mid brain (2), and bilateral cerebellar hemisphere (3) (at the slice level with the maximum cerebellar hemisphere), thalami (4), basal ganglia (5), and lower frontal (7), mid temporal (8), mid frontal (9), occipital (10), upper frontal (11), and parietal cortices (12). The MRI showed nodular high intensity lesions in the bilateral caudate, putamina and thalami on T2WI.



## 2. Material and methods

### 2.1. Patients (Table 1)

This study enrolled five patients (four males, one female) who have been followed at the Tohoku University Hospital and Takuto Rehabilitation Center for Children. Table 1 lists the clinical features, MRI findings, results of genetic testing as well as FDG-PET findings. The median age of onset was 2 (range 1–6) years. The median age at the FDG-PET study was 11 (range 4–13) years. There was a wide range of evaluation period from the onset, which reflects the different timing of referrals of patients to our tertiary hospital. T2 weighted brain MRI showed high-intensity areas in the putamen bilaterally in five patients, caudate bilaterally in four, thalamus bilaterally in two, and brainstem in one. Cerebellar atrophy was observed in older two patients. All patients were taking high-dose vitamins, including vitamin B<sub>1</sub> (five patients), vitamin C (two patients), biotin (four patients), and coenzyme Q10 (three patients). Two patients were taking levodopa/carbidopa and one dichloroacetate. One patient was taking anticonvulsants. All patients showed elevated levels of lactate and pyruvate in the cerebrospinal fluid and blood. Four patients underwent gene analysis, which revealed reported mitochondrial DNA mutations (m.T8993G in two, m.T14887C in one, and m.T10191C in one). As disease controls, seven epilepsy patients (median age 10 (range 6–16) years) who had normal MRI and FDG-PET studies were selected. The clinical FDG-PET study was performed on these patients because seizure

control was not achieved at this period, and the results were ascertained as normal by both radiologist and pediatric neurologist. The effects of antiepileptic drugs on the FDG-PET scans were considered as minimum in these patients.

### 3. Methods

Positron emission tomography was performed 1 h after administering 3.1 MBq/kg <sup>18</sup>F-FDG (minimum 74 MBq) using a Biograph Duo PET/CT scanner (Siemens, Hoffman Estates, IL) after at least a 4-h fast with intravenous midazolam sedation. There were no side effects of sedation. Emission scans of the brain were performed for 10 min. For semiquantitative analysis of lesions with decreased <sup>18</sup>F-FDG uptake, the mean standard uptake value (SUV) based on body weight (g) was calculated in each brain structure in each axial slice and converted into a value based on lean body mass [10]:

$$\text{SUV} = \text{tissue activity concentration (Bq/mL)} / [\text{administered activity (Bq)} / \text{weight (g)}].$$

Oval regions of interest (ROIs) were placed by a well-trained nuclear physician (T.K.) on the pons, mid brain, and bilateral cerebellar hemispheres (at the slice level with the maximum cerebellar hemisphere), thalami, basal ganglia, and the lower temporal, lower frontal, mid temporal, mid frontal, occipital, upper frontal, and parietal cortices (Fig. 1). ROIs were carefully selected in each patient to minimize localization bias between patients. Each ROI was subdivided into nine segments:

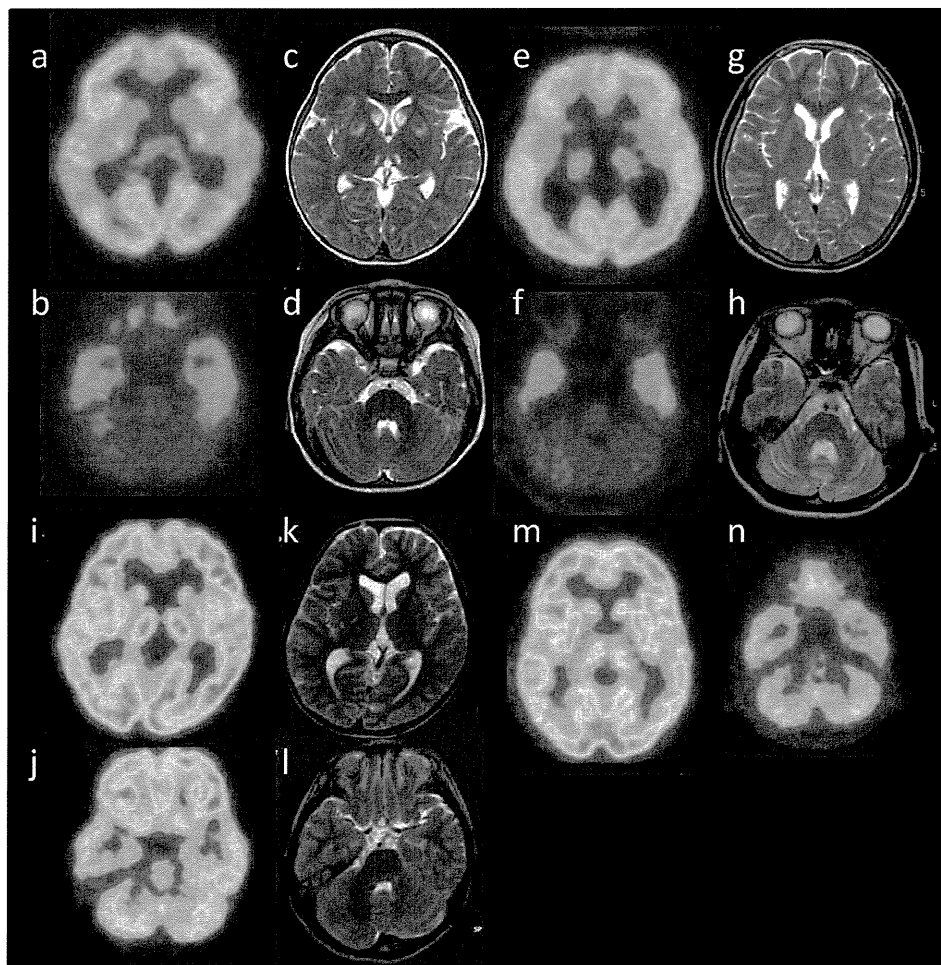


**Fig. 2.** Results of FDG-PET study in patients with Leigh syndrome. The images of FDG-PET (a–b, e–f, i–j, m–n) and MRI (T2WI) (c–d, g–h, k–l) of patient 1 (a–d), patient 4 (e–h) and patient 2 (i–l) and disease control (m–n) were shown. The glucose up take was reduced in the cerebellum in patients 1 and 4, bilateral basal ganglia in patient 1, 2 and 4, and temporal lobes in patients 1 and 4. The cerebellar hypometabolism was observed even in a patient whose MRI showed no abnormalities (a–d).

frontal (6 ROIs/person), temporal (4 ROIs/person), parietal (2 ROIs/person), occipital (2 ROIs/person), thalamus (2 ROIs/person), basal ganglia (2 ROIs/person), mid brain (1 ROI/person), pons (1 ROI/person), and cerebellum (2 ROIs/person). We compared the SUV of the nine

segments, which were the average of ROIs in each region, between the patients with Leigh syndrome and disease controls. Statistical analysis was carried with Mann–Whitney’s *U* test. Significance was set as  $p < 0.05$ .

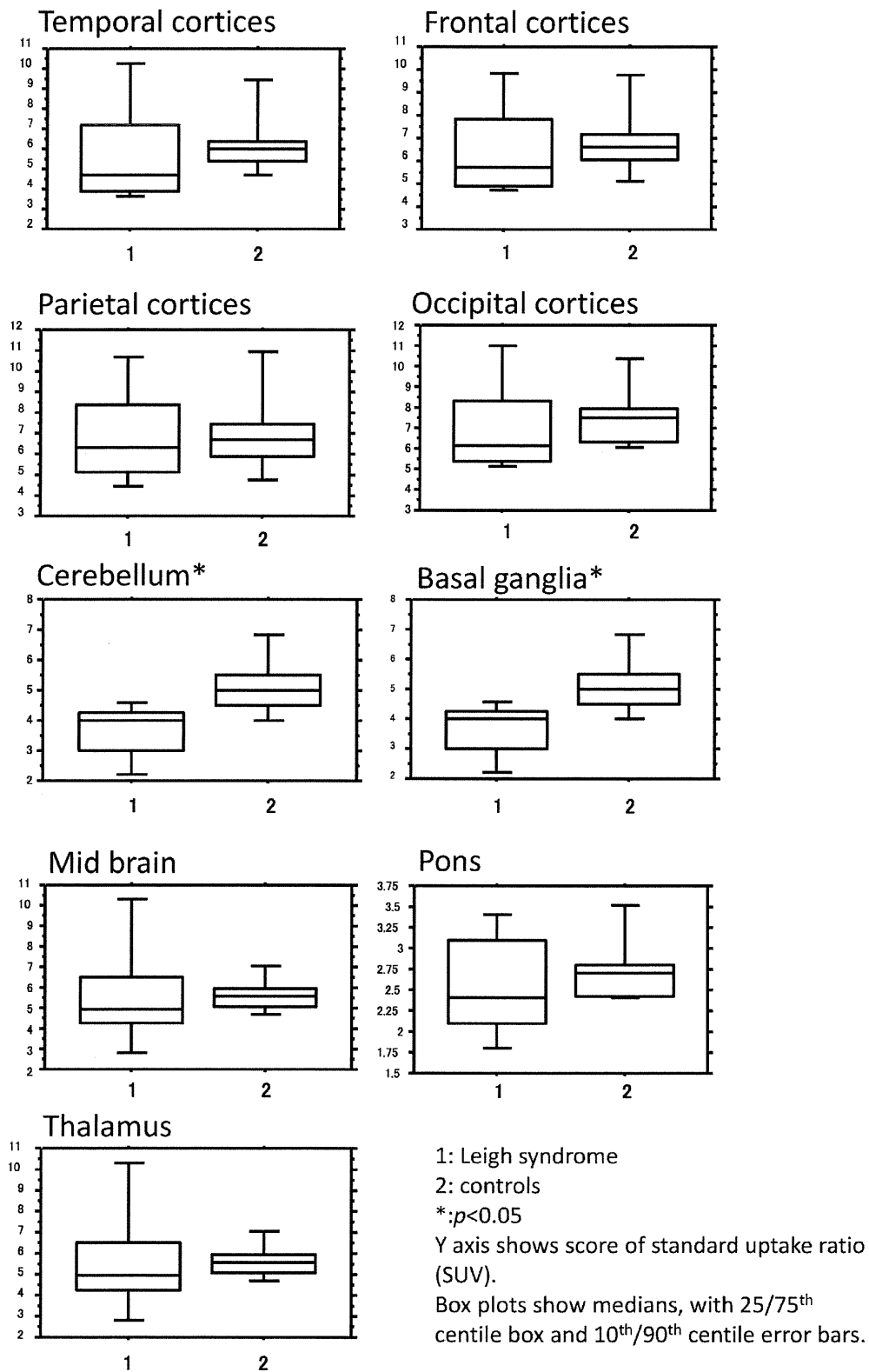


**Fig. 3.** Results of the statistical analysis of the SUV compared to the disease controls. In patients with Leigh syndrome, glucose uptake was decreased significantly in the cerebellum and basal ganglia.

This study was approved by the Ethics Committee of Tohoku University Hospital. Written informed consent on research PET scans was obtained from the patients' families after a thorough explanation.

#### 4. Results (Table 1, Figs. 2, 3)

The glucose up take of cerebellum was reduced in three patients, bilateral thalami in three, bilateral basal ganglia in five, bilateral temporal lobes in three and left frontal lobe in one. The cerebellar hypometabolism was observed even in patients whose MRI showed no abnormalities. The all patients with cerebellar hypometabolism showed clinically evident ataxia. Dystonia was observed in two patients at FDG-PET study although hypometabolism of the basal ganglia was observed in all patients. As compared to the disease control, glucose uptake was decreased significantly in the cerebellum and basal ganglia in patients with Leigh syndrome.

#### 5. Discussion

There are no effective treatment protocols for Leigh syndrome. To develop an effective drug regimen, a standardized evaluation method is essential. Previous studies used clinical scales such as the Newcastle Pediatric Mitochondrial Disease Scale (NPMDS) [11] and HMPAO-SPECT [8–9]. Of note, Blankenberg et al. reported that brain perfusion was decreased in patients with Leigh syndrome, especially in the basal ganglia, cerebellum and cortex. After a 3-month trial of a new agent, a correlation between the perfusion changes in the cerebellum and improvement in the NPMDS score was seen [8]. Previously, we reported a patient with Leigh syndrome who was treated with idebenone, the efficacy of which was evaluated with blood gas analysis, respirogram, and a neurophysiological analysis [12].

The present study demonstrated significantly hypoactive glucose metabolism in the cerebellum and basal ganglia, which could explain the ataxia and dystonia in patients with Leigh syndrome. However, the correlation between regions of hypoactive glucose metabolism and clinical symptoms was not clear except for ataxia and cerebellar hypometabolism, which needs further elucidation using a larger sample size. The cerebellar hypometabolism was observed even in patients whose MRI showed no abnormalities. This fact implies that FDG-PET may have superior sensitivity at visualizing dysfunctional structures in the brain. FDG-PET may be useful to understand the pathogenesis of stroke-like episodes in patient with mitochondrial encephalopathy, lactic acidosis, and stroke-like episodes (MELAS) [13]. Ikawa et al. postulated that oxidative stress following hyperemia along with increased glucose metabolism play crucial roles in the pathogenesis of MELAS stroke-like episodes [13]. Molnar et al. also reported decreased cerebral glucose uptake, especially in the occipital and temporal lobes in patients with mitochondrial myopathy and neuropathy, chronic progressive external ophthalmoplegia (CPEO), and MELAS [14]. They showed that there is no correlation between the decreased glucose metabolism and the duration of the disease.

There were several limitations to this study. First, the ROIs were placed manually, which means there are many unmeasured broad regions outside the ROIs. This needs to be reconsidered with a fully automated ROI analysis. For more appropriate analysis, statistical parametric mapping (SPM) would have been validated the present results, which remains to be carried out. In addition, the high-dose vitamins and other drugs the patients were taking might have affected the results. Finally, the sample size was small.

Nevertheless, we believe that FDG-PET might be useful for evaluating the brain dysfunction and treatment efficacy of new drugs in patients with Leigh syndrome. Further study with more patients using

advanced methods to quantify the glucose uptake is needed before drawing a conclusion.

#### Contributors

Kauzhiro Haginoya, Tomohiro Kaneta, Noriko Togashi, Naomi Hino-Fukuyo, Tomoko Kobayashi, Mitsugu Uematsu, Taro Kitamura, Takehiko Inui, Yukimune Okubo, Yusuke Takezawa, Mai Anzai and Wakaba Endo performed clinical work-ups and sample collection. Noriko Miyake, Hiroto Saito, and Naomichi Matsumoto provided genetic analyses. Kauzhiro Haginoya, Tomohiro Kaneta and Shigeo Kure conceived and coordinated the study and wrote the manuscript.

#### Acknowledgements

This study was supported by: the Japanese Ministry of Health, Labour, and Welfare; a Grant-in-Aid for Scientific Research (A) (13313587); the Takeda Science Foundation; the fund for Creation of Innovation Centers for Advanced Interdisciplinary Research Areas Program in the Project for Developing Innovation Systems; the Strategic Research Program for Brain Sciences (11105137); and a Grant-in-Aid for Scientific Research on Innovative Areas (Transcription Cycle) from the Japanese Ministry of Education, Culture, Sports, Science, and Technology (N.M.) and the Japan Society for the Promotion of Science (a Grant-in-Aid for Scientific Research (B)) (25293085); the Takeda Science Foundation (H.S.)

#### References

- [1] N. Darin, A. Oldfors, A.R. Moslemi, E. Holme, M. Tulinius, The incidence of mitochondrial encephalomyopathies in childhood: clinical features and morphological, biochemical, and DNA abnormalities, *Ann. Neurol.* 49 (2001) 377–383.
- [2] D. Leigh, Subacute necrotizing encephalomyelopathy in an infant, *J. Neurol. Neurosurg. Psychiatry* 14 (1951) 216–221.
- [3] S. Rahman, R.B. Blok, H.H. Dahl, D.M. Danks, D.M. Kirby, C.W. Chow, et al., Leigh syndrome: clinical features and biochemical and DNA abnormalities, *Ann. Neurol.* 39 (1996) 343–351.
- [4] K. Sofou, K. Steneryd, L.M. Wiklund, M. Tulinius, N. Darin, MRI of the brain in childhood-onset mitochondrial disorders with central nervous system involvement, *Mitochondrion* 13 (2013) 364–371.
- [5] K. Sofou, I.F. De Co, P. Isohanni, E. Ostergaard, K. Naess, L. De Meirleir, et al., A multicenter study on Leigh syndrome: Disease course and predictors of survival, *Orphanet. J. Rare Dis.* 9 (2014) 52.
- [6] K. Yanai, K. Jinuma, T. Matsuzawa, M. Ito, S. Miyabayashi, K. Narisawa, et al., Cerebral glucose utilization in pediatric neurological disorders determined by positron emission tomography, *Eur. J. Nucl. Med.* 13 (1987) 292–296.
- [7] T.C. Yen, S.H. Yeh, 99mTc-HMPAO brain single photon emission computerized tomography in mitochondrial encephalomyopathies, *Zhonghua Yi Xue Za Zhi (Taipei)* 56 (1995) 287–291.
- [8] F.G. Blankenberg, S.L. Kinsman, B.H. Cohen, M.L. Goris, K.M. Spicer, S.L. Perlman, et al., Brain uptake of Tc99m-HMPAO correlates with clinical response to the novel redox modulating agent EPI-743 in patients with mitochondrial disease, *Mol. Genet. Metab.* 107 (2012) 690–699.
- [9] G.M. Enns, S.L. Kinsman, S.L. Perlman, K.M. Spicer, J.E. Abdenur, B.H. Cohen, et al., Initial experience in the treatment of inherited mitochondrial disease with EPI-743, *Mol. Genet. Metab.* 105 (2012) 91–102.
- [10] K. Jingu, T. Kaneta, K. Nemoto, A. Ichinose, M. Oikawa, Y. Takai, et al., The utility of <sup>18</sup>F-fluorodeoxyglucose positron emission tomography for early diagnosis of radiation-induced myocardial damage, *Int. J. Radiat. Oncol. Biol. Phys.* 66 (2006) 845–851.
- [11] C. Phoenix, A.M. Schaefer, J.L. Elson, E. Morava, M. Bugiani, G. Uziel, et al., A scale to monitor progression and treatment of mitochondrial disease in children, *Neuromuscul. Disord.* 16 (2006) 814–820.
- [12] K. Haginoya, S. Miyabayashi, M. Kikuchi, A. Kojima, K. Yamamoto, K. Omura, et al., Efficacy of idebenone for respiratory failure in a patient with Leigh syndrome: a long-term follow-up study, *J. Neurol. Sci.* 278 (2009) 112–114.
- [13] M. Ikawa, H. Okazawa, K. Arakawa, T. Kudo, H. Kimura, Y. Fujibayashi, et al., PET imaging of redox and energy states in stroke-like episodes of MELAS, *Mitochondrion* 9 (2009) 144–148.
- [14] M.J. Molnar, A. Valikovics, S. Molnar, L. Tron, P. Dioszeghy, F. Mechler, et al., Cerebral blood flow and glucose metabolism in mitochondrial disorders, *Neurology* 55 (2000) 544–548.

# 研究班員名簿

ミトコンドリア病の調査研究班

区 分	氏 名	所 属 等	職 名
研 究 代 表 者	後藤雄一	国立精神・神経医療研究センター神経研究所疾病研究第二部	部長
研 究 分 担 者	小坂 仁	自治医科大学小児科	教授
	大竹 明	埼玉医科大学小児科	教授
	北風政史	国立循環器病研究センター病院・研究開発基盤センター	部長
	古賀靖敏	久留米大学医学部小児科	教授
	小牧宏文	国立精神・神経医療研究センター病院臨床研究推進部・小児神経学	部長
	佐野 輝	鹿児島大学学術研究院医歯学域医学系精神機能病学	教授
	末岡 浩	慶應義塾大学医学部産婦人科	准教授
	田中雅嗣	東京都健康長寿医療センター臨床検査科	部長
	三牧正和	帝京大学医学部附属病院小児科	准教授
	山岨達也	東京大学医学部耳鼻咽喉科	教授
	米田 誠	福井県立大学看護福祉学部	教授
研 究 協 力 者	太田成男	日本医科大学大学院医学研究科	教授
	岡崎康司	埼玉医科大学・ゲノム医学研究センター	教授・所長
	金田大太	東京都健康長寿医療センター神経内科	医長
	木村 円	国立精神・神経医療研究センター トランスレーショナル・メディカルセンター臨床研究支援部	室長
	杉本立夏	国立精神・神経医療研究センター病院遺伝カウンセリング室	遺伝カウンセラー
	砂田芳秀	川崎医科大学医学部神経内科	教授
	須藤 章	楡の会こどもクリニック	医長
	竹下絵里	国立精神・神経医療研究センター病院小児神経診療部	医員
	中野和俊	東京女子医科大学病院小児科	非常勤講師
	西野一三	国立精神・神経医療研究センター神経研究所疾病研究第一部	部長
	中川正法	京都府立医科大学附属北部医療センター	病院長
	中村 誠	神戸大学大学院医学系研究科外科系講座眼科学	教授
	萩野谷和裕	拓桃医療療育センター・東北大学医学部小児科	センター長・臨床教授
	村山 圭	千葉県こども病院代謝科	主任医長
事 務 局	大科京子	〒187-8502 東京都小平市小川東町 4-1-1 国立精神・神経医療研究センター神経研究所 疾病研究第二部 T E L 042-346-1713 F A X 042-346-1743 e-mail ohshina@ncnp.go.jp	事務員
経 理 事 務 担 当 者	松田敏宏	〒187-8551 東京都小平市小川東町 4-1-1 T E L 042-341-2712 (内線2157) F A X 042-346-1425 e-mail t-matsuda@ncnp.go.jp	財務経理部 財務経理課 第二契約係長